

Geometrically Constrained Statistical Models on Fixed and Random Lattices: From Hard Squares to Meanders

P. Di Francesco¹

*CEA-Saclay, Service de Physique Théorique,
F-91191 Gif sur Yvette Cedex, France*

We review various combinatorial applications of field theoretical and matrix model approaches to equilibrium statistical physics involving the enumeration of fixed and random lattice model configurations. We show how the structures of the underlying lattices, in particular their colorability properties, become relevant when we consider hard-particles or fully-packed loop models on them. We show how a careful back-and-forth application of results of two-dimensional quantum gravity and matrix models allows to predict critical universality classes and consequently exact asymptotics for various numbers, counting in particular hard object configurations on fixed or random lattices and meanders.

¹ philippe@spht.saclay.cea.fr

1. Introduction

Physics provides a source of alternative approaches to well-posed mathematical problems, allowing sometimes for less rigorous but more predictive results, such as those discussed in these notes. The reason is that the tools employed are often somewhat ill-defined from a purely mathematical point of view, although they are often validated by experiment. In every physicist's toolbox, field theory is certainly the most powerful one, as it basically allows for an effective description of the essential behavior and properties of the situations it models.

Our main concern here will be with solving well-posed combinatorial problems by means of physical approaches and reasoning. This type of approach must have a sort of exotic flavor when observed from a purely mathematical point of view. The very principles it relies on borrow from the developments of field theory, such as renormalization group techniques applied to critical phenomena. Instead of trying to be completely exhaustive, which would go far beyond the scope of the present notes, we will rather try to extract the essentials and main lessons of the field-theoretical approaches. We will also present some alternative techniques such as matrix integrals allowing to address some of these combinatorial problems.

The questions we will be considering here deal with fixed or random statistical two-dimensional lattice models, used to describe two-dimensional interfaces as well as discrete two-dimensional quantum gravity (2DQG). Combinatorially, these are simply problems of enumeration of configurations involving either decorated lattices or decorated graphs. More precisely, we will discuss here two classes of models for which the details of the underlying lattice are important: these models “feel” strongly their underlying discretized space. They are the hard-particle and fully-packed loop models. We will be mainly interested in understanding the critical behavior of these systems, namely in locating phase transitions in the space of parameters where thermodynamic quantities, characteristic of the collective behavior of the system at large size, become singular. As we will explain, these singularities fall into “universality classes” described by various field theories, and characterized by critical exponents governing their algebraic singularities.

The first theory describes objects (particles) occupying the vertices of the lattice, with a nearest neighbor exclusion constraint that no two vertices connected by an edge may be simultaneously occupied. Despite the local character of this constraint, it allows for the particles to “feel” the details of the lattice. When for instance we increase the density

of occupation up to its maximum, particles will try to occupy every other vertex in the lattice, thus will feel for instance whether it is bipartite or not.

The second theory describes loops occupying edges of the lattice, with the additional constraint that every vertex is visited by a loop. Again, the bipartite (or not) character of the lattice will prove crucial in the discussion of the critical behavior of the system.

While solving the first theory will eventually lead to the exact enumeration of random planar graphs with hard-particles on them, solving the second one will lead to an asymptotic solution of the so-called “meander” problem of enumeration of the topologically inequivalent configurations of a closed road crossing a river through a given number of bridges. The materials collected in this review article include in particular Refs. [1] and [2], where random lattice hard-particle and meander problems were first solved (see also the review article [3]).

The paper is organized as follows. In Sect. 2, we collect a few definitions and results regarding the thermodynamics of two-dimensional statistical lattice models on fixed and random lattices, including in particular field-theoretical ones. Sect. 3 is devoted to the study of hard particles on various random lattices, in the form of planar graphs with fixed valence. We show in particular how another favorite physicist’s tool, the matrix integral, may be used to completely solve various enumeration problems involving decorated graphs. When applied to hard particles, these allow for a complete understanding of the crystallization transition, namely a critical value of the density of occupation below which the system is fluid (particles occupy vertices quasi-randomly) and beyond which a crystal of particles forms. We show however that such a transition only exists on (fixed or random) lattices with a colorability property allowing for the existence of maximally occupied sublattices. The critical behavior is then traced back directly to the existence and structure of these sublattices. We show in particular that for bipartite lattices, the critical transition lies in the universality class of the critical 2D Ising model, thus proving on a random lattice some old fixed lattice conjectures concerning hard squares or hard triangles [4] [5] [6]. In Sect. 4, we address fully-packed loop models on fixed and random lattices. After recalling some known results in the fixed lattice case, we move to random lattices. Remarkably, just like in the hard-particle case, we find that according to whether the random lattices are bipartite or not, the critical universality class predicted is different. By suitably following a two-flavor fully-packed loop model from its fixed lattice version to its random lattice one, we arrive at the identification of the universality class for meanders, which allows in particular to predict the meander configuration exponent $\alpha = \frac{29+\sqrt{145}}{12}$, governing the

large n asymptotics of the meander number with $2n$ bridges $M_{2n} \sim g_c^{-2n}/n^\alpha$. We gather a few concluding remarks in Sect. 5, as well as another simple prediction, as a challenge for mathematicians to prove.

2. 2D Quantum Gravity and Asymptotic Graph Combinatorics

2.1. 2D Lattice Models

The archetypical systems studied in 2D equilibrium statistical mechanics are lattice models, whose configurations are defined as maps σ from, say the vertices i of a 2D lattice \mathcal{L} (or more precisely a finite connected subset thereof say of rectangular shape of size $L \times T$, denoted by $\mathcal{L}_{L,T}$, and with definite, say periodic boundary conditions) to a target space \mathcal{T} usually real. The model is further defined through an energy functional $E(\sigma)$, and each configuration is attached a statistical weight proportional to $e^{-\beta E(\sigma)}$, where $\beta = 1/(k_B T)$, k_B the Boltzmann constant and T the temperature. One is usually interested in the properties of global functions such as the partition function

$$Z_{L,T} = \sum_{\sigma} e^{-\beta E(\sigma)} \quad (2.1)$$

where the sum extends over the set of maps from $\mathcal{L}_{L,T}$ to \mathcal{T} . This is precisely the normalization of the probability $p(\sigma) = e^{-\beta E(\sigma)}/Z_{L,T}$ of the configuration σ . This probability weight allows to answer various questions regarding correlations in the system, through the corresponding expectation value denoted generically by $\langle \dots \rangle = \sum_{\sigma} \dots p(\sigma)$.

As a simple illustration, the Ising model has $\mathcal{T} = \{-1, +1\}$, and the images $\sigma(i)$ are used for instance to describe the spins (magnetic moments) in metals. The functional energy usually incorporates some information on interactions within the system or with some external fields or forces. For the Ising model, it reads $E(\sigma) = -J \sum_{(i,j)} \sigma(i)\sigma(j) - H \sum_i \sigma(i)$, where the first sum extends over nearest neighboring pairs of vertices (i, j) and expresses ferro- ($J > 0$) or antiferro- ($J < 0$) magnetic interactions, while the second sum expresses the coupling of the system to an external magnetic field H . In general, the energy functional depends on external parameters (such as βJ and βH in the Ising case).

The archetypical questions one tries to answer involve the thermodynamic limit in which the system becomes large, say $L, T \rightarrow \infty$ with L/T finite, and on its dependence on the external parameters. In this limit, thermodynamic functions such as $Z = \lim(Z_{L,T})^{\frac{1}{LT}}$

may develop singularities when the parameters approach some critical values, corresponding to phase transitions and critical phenomena. Of particular interest are those in which a divergence occurs for the length characteristic of the effective range of interactions, the *correlation length*. The corresponding critical singularities fall into so-called universality classes, characterized by scaling exponents which govern the leading algebraic behavior of the singular part of the thermodynamic functions of the system. For instance, in the ferromagnetic Ising model with vanishing magnetic field, one defines a “thermal” exponent α , characteristic of the leading singularity of the free energy $F = \text{Log } Z$ when the temperature T approaches a critical value T_c :

$$F|_{\text{sing}} \propto |T - T_c|^{2-\alpha} \quad (2.2)$$

Similarly, at $T = T_c$, we also get a singular behavior for F when we switch on a small magnetic field H , with

$$F|_{\text{sing}} \propto |H|^{2-\beta} \quad (2.3)$$

which defines the “magnetic susceptibility” exponent β . The exponents α, β are expected to be more universal than the actual value of the critical temperature T_c : indeed, one finds for instance that T_c depends on the precise type of lattice on which the model is defined, while α, β only depend on its dimensionality.

In two dimensions, it has been shown that under some assumption of locality of the interactions, critical singularities corresponding to the divergence of the correlation length fall into universality classes described by two-dimensional conformal field theories (CFT), upon taking the continuum critical limit of the models, in which we let at the same time the size of the system tend to infinity and the lattice spacing tend to zero while parameters tend to critical values, so that the lattice becomes the two-dimensional plane (or a higher genus Riemann surface according to boundary conditions), and configuration maps become fields. Conformal invariance of the resulting field theory is directly linked to the divergence of the correlation length which implies in particular local scale invariance of the theory. Two-dimensional CFT’s have been extensively studied and partly classified, providing us with a sort of Mendeleviev table of universality classes of critical phenomena in two dimensions, in the form of a list of critical exponents (see the text [7] and references therein). More precisely, CFT’s are characterized by their central charge $c_m = 1 - 6/(m(m+1))$ and the conformal dimensions of their operators $h_{r,s} = (((m+1)r - ms)^2 - 1)/(4m(m+1))$ respectively the central extension and highest weights of the corresponding representations

of the Virasoro algebra, m some complex parameter, and r, s some positive integers, further restricted to a finite set in the case of minimal models, where m is rational. The conformal dimensions govern the fall-off with distance of correlation functions. For instance we have for a conformal operator Φ_h of dimension h : $\langle \Phi_h(z, \bar{z}) \Phi_h(0, 0) \rangle = 1/|z|^{4h}$. Upon identifying the operators of the theory as generating perturbations of the various parameters away from their critical values, one may relate the corresponding critical exponents to their conformal dimension through²

$$\alpha = \frac{1 - 2h}{1 - h} \quad (2.4)$$

For instance, the critical 2D Ising model corresponds to a CFT with $m = 3$, i.e. $c = 1/2$ and the thermal operator associated with perturbations in the temperature has $h_{1,3} = 1/2$, so that the thermal exponent is $\alpha = 0$ (in this case, the singularity is weaker and involves the logarithm of $|T - T_c|$). Besides, the magnetic “spin” operator, the continuous version of the map σ , has conformal dimension $h_{2,2} = 1/16$, which leads to the magnetic susceptibility exponent $\beta = 14/15$.

A number of classifications of CFT’s are now available, the most remarkable of which is probably that of “minimal models” with central charges $c < 1$, namely CFT’s with a finite number of conformal primary fields [8]. They turn out to have central charges $c = c(p, q) \equiv 1 - 6(p - q)^2/(pq)$, indexed by two coprime positive integers p and q . The constraint of unitarity (positivity of correlators, and in particular positivity of the probabilities $p(\sigma)$) further restricts q and p to obey $|p - q| = 1$. In this language, the Ising model corresponds to $p = 3, q = 4$.

2.2. 2D Random Lattice Models

In this work, we consider random lattice models, defined in precisely the same way as ordinary lattice models, but by replacing the underlying lattice by a somewhat arbitrary possibly disconnected tessellation of the plane (or higher genus surface). The tessellation becomes therefore part of the configuration to be summed over (see Fig. 1 for an illustration). This was introduced as a discrete model of 2D quantum gravity (2DQG), namely to describe the coupling of some statistical “matter” models to the quantum fluctuations of

² This is done by dimensional analysis. Writing the corresponding perturbation of the conformal action functional as $(t - t_c) \int d^2z \Phi_h(z, \bar{z})$, and performing a local rescaling $z \rightarrow \lambda z$, we find that $(t - t_c) \sim \lambda^{2h-2}$ as the action is dimensionless. The thermodynamic free energy $F = \lim_{\frac{1}{LT}} \text{Log } Z_{L,T}$ however is per unit of area, hence $(t - t_c)^{2-\alpha} \sim \lambda^{-2}$, hence $\alpha = 1/(1 - h)$.

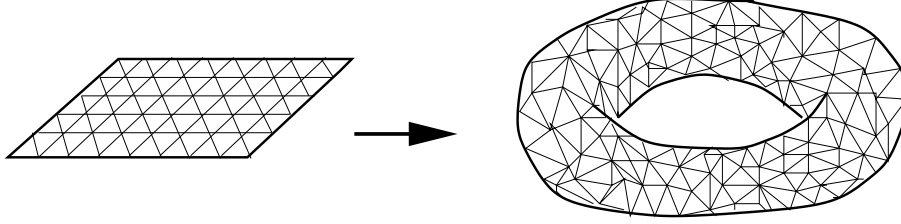


Fig. 1: Schematic representation of how we go from a 2D statistical lattice model (defined here on a finite portion of the triangular lattice) to a random lattice model, in which the lattice is replaced by arbitrary tessellations of space (here a random triangulation tessellating a genus one surface).

the underlying “space”, represented by random lattices or tessellations (see e.g. Ref. [9] for a review and more references). For each tessellation Θ , we associate a statistical weight directly borrowed from the Einstein action in 2D, namely a weight $N^{\chi(\Theta)} g^{A(\Theta)}$ where χ and A are respectively the Euler characteristic and area of the tessellation (respectively measured via $\chi = \#\text{faces} - \#\text{edges} + \#\text{vertices}$ and $A = \#\text{tiles}$), and where N and g are the discrete counterparts of the Newton constant and cosmological constant. For each tessellation Θ together with a spin configuration $\sigma : \Theta \rightarrow \mathcal{T}$ on it, we also have a weight $e^{-\beta E(\sigma)}$ and we must divide by the order of the automorphism group $|Aut(\Theta, \sigma)|$. This leads for instance to the discretized partition function of any 2D statistical lattice model coupled to 2D quantum gravity

$$Z = \sum_{\text{tessel. } \Theta} N^{\chi(\Theta)} g^{A(\Theta)} \sum_{\substack{\text{config.} \\ \sigma: \Theta \rightarrow \mathcal{T}}} e^{-\beta E(\sigma)} / |Aut(\Theta, \sigma)| \quad (2.5)$$

Note that the parameter N allows to isolate the contributions of tessellations of fixed genus. In the following we will be mainly interested in the genus zero contributions, obtained by letting $N \rightarrow \infty$. Note also that the free energy $F = \text{Log } Z$ selects only the connected tessellations in the sum (2.5).

Like in the fixed lattice case, we are interested in the thermodynamic limit of the system, in which say the average area or some related quantity diverges, ensuring that the dominant contributions to Z e.g. come from large tessellations. This is guaranteed in general by the existence of a critical value g_c of the cosmological constant g at which such singularities take place. This value is a priori a function of the type of random lattices we sum over as well as of the various matter parameters. We may now attain interesting critical points by also letting the matter parameters approach critical values, a priori distinct from those on fixed lattices. The result is well described by the coupling

of the corresponding CFT's with quantum fluctuations of space, namely by letting the metric of the underlying 2D space fluctuate. Such fluctuations may be represented in the conformal gauge by yet another field theory, the Liouville field theory, which is coupled to the matter CFT. This field theoretical setting allows for a complete understanding of the various critical exponents occurring at these critical points [21]. For instance, one defines the (genus zero) string susceptibility exponent γ_{str} as the exponent α associated to the cosmological constant singularity, namely by writing the singularity of the free energy as

$$F|_{\text{sing}} \propto (g_c - g)^{2-\gamma_{str}} \quad (2.6)$$

In the case of coupling of a matter theory with central charge c to 2DQG, one has the exact relation [21]

$$\gamma_{str} = \frac{c - 1 - \sqrt{(1-c)(25-c)}}{12} \quad (2.7)$$

In the case of “pure gravity”, namely when the matter is trivial and has $c = 0$, we get $\gamma_{str} = -1/2$, while for the critical Ising model with $c = 1/2$ we have $\gamma_{str} = -1/3$.

Upon coupling to gravity the operators of the CFT ($\Phi_h(z, \bar{z})$) get “dressed” by gravity ($\Phi_h \rightarrow \tilde{\Phi}_h \equiv \Psi_\Delta$) and acquire dressed dimensions Δ , given similarly by [21]

$$\Delta = \frac{\sqrt{1-c+24h} - \sqrt{1-c}}{\sqrt{25-c} - \sqrt{1-c}} \quad (2.8)$$

As opposed to the fixed lattice case, where conformal dimensions govern the fall-off of correlation functions of operators with distance, the dressed operators of quantum gravity do not feel distances, as their position is integrated over the surfaces, but rather only feel changes of area at fixed genus. More precisely the general genus zero correlators behave in the vicinity of g_c [21] as

$$\langle \Psi_{\Delta_1} \Psi_{\Delta_2} \dots \Psi_{\Delta_n} \rangle \sim (g_c - g)^{2-\gamma_{str} + \sum_{1 \leq i \leq n} (\Delta_i - 1)} \quad (2.9)$$

These results may be easily translated into the large (but fixed) area A behavior of the various thermodynamic quantities, upon performing a Laplace transform, which selects the coefficient of g^A in the various expansions. Let F_A denote the partition function for connected tessellations of genus zero and area A , we have

$$F_A \sim \frac{g_c^{-A}}{A^{3-\gamma_{str}}} \quad (2.10)$$

while if $\langle \dots \rangle_A$ denotes any genus zero correlator at fixed area, we have

$$\langle \Psi_{\Delta_1} \Psi_{\Delta_2} \dots \Psi_{\Delta_n} \rangle_A \sim \frac{g_c^{-A}}{A^{3-\gamma_{str} + \sum_{1 \leq i \leq n} (\Delta_i - 1)}} \quad (2.11)$$

In [21], all these formulas were also generalized to higher genus as well.

As an illustration of eqn. (2.10), recall that the number of quadrangulations of the sphere with A square tiles and with a marked edge (dually equal to the number of rooted tetravalent planar maps with A vertices) reads [19]

$$N_A = \frac{3^A}{2(A+1)(A+2)} \binom{2A}{A} \sim \frac{12^A}{A^{5/2}} \quad (2.12)$$

Noting that the rooting simply amounts to $N_A \propto A F_A$, the asymptotics (2.12) correspond to $g_c = 1/12$ and $\gamma_{str} = -1/2$, hence $c = 0$. This is one of the various ways to attain the universality class of pure gravity, namely by summing over bare tessellations without matter on them.

So far so good, basically all asymptotic combinatorics problems involving planar (or more generally fixed genus) graphs seem to be solved via eqns. (2.10) and (2.11) or their higher genus generalizations, provided one is able to identify the central charge c of the underlying CFT. This latter step however may prove to be quite involved. In fact, the aim of this note is to clarify a large class of cases for which the naive application of these formulas would lead to the wrong result. These are statistical models whose definition strongly relies on the structure of the underlying (fixed or random) lattice. This is the case for hard particles, as well as for fully-packed loops, the two main subjects of this note.

3. Hard Particles

The first class of problems we will be discussing is that of hard particles occupying or not the vertices of the fixed or random lattices, and subject to the “hardness” or particle-exclusion constraint that no two adjacent vertices may be simultaneously occupied. One usually attaches an activity z per occupied vertex. In this section, we first recall the fixed lattice results, and display the exact or predicted critical behavior of the model. Generically it undergoes a crystallization transition between a disordered phase of low-density of occupation and a crystalline phase of maximal occupancy. We next turn to the exact solution of the same model on some random lattice, only to discover that the crystalline transition is wiped out by the sum over lattices. To solve this puzzle, we simply

notice that the transition can take place only if the random lattices allow for the existence of some generic crystalline configurations. We finally show that the model, when defined on random *bipartite* lattices, has a crystalline transition in the universality class of the two-dimensional critical Ising model coupled to 2DQG.

3.1. Fixed lattice results and conjectures

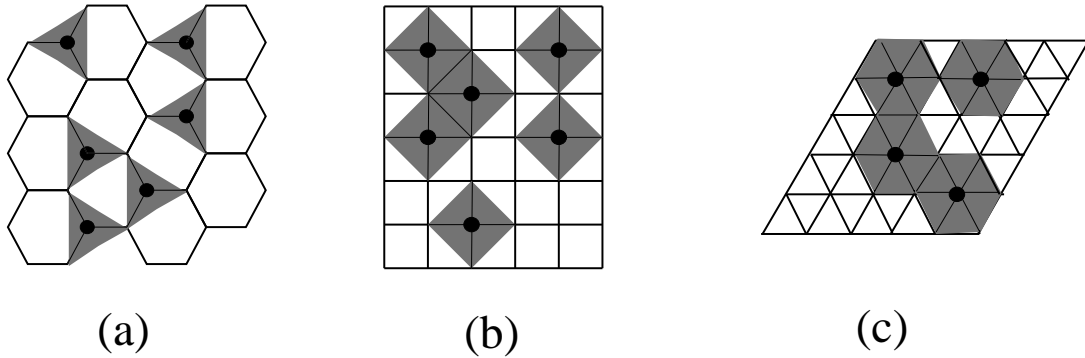


Fig. 2: Typical configurations of hard particles on the (a) hexagonal, (b) square and (c) triangular lattices. We have also represented in grey the excluded area translating the nearest neighbor exclusion into a non-overlapping constraint of tiles. Their respective shapes are triangles, squares and hexagons, hence the names hard triangles, squares or hexagons.

Hard particle models have been extensively studied in the physics literature, under various names: hard-core lattice gas, nearest-neighbor exclusion models, etc ... [4] [5] [6] [10] [11]. Among the host of results and conjectures, let us mention the three cases of the hexagonal, square and triangular lattices. The corresponding models are also often referred to as hard triangle, square or hexagon models, as in the dual picture an occupied vertex may be replaced by some tile whose shape transforms the hard-particle constraint into a no-overlap condition between tiles (see Fig. 2 for an illustration in the hexagonal (a), square (b) and triangular (c) cases, respectively corresponding to hard triangles, squares and hexagons). In the three cases, one expects in the thermodynamic limit a crystallization transition to take place at some critical value $z = z_+ > 0$ between a low- z disordered phase and a high- z crystalline phase in which, when $z \rightarrow \infty$, only one of a few available “groundstates” are realized, namely some maximally occupied configurations, in which the particles occupy a sublattice of the original one. For the hexagonal and square cases, where the lattice is bipartite, there are exactly *two* such crystalline groundstates, as opposed to

the triangular case, where there are *three*. In addition, one expects as well some “non-physical” critical point at some other value $z = z_- < 0$, independent of the precise details of the lattice, and generically described by the Yang-Lee edge singularity [12] (of the Ising model in the presence of a critical imaginary electric field).

The triangular lattice case is particularly interesting, as it proved to be exactly solvable by Baxter [10], who explicitly worked out various critical exponents characterizing the crystallization transition. He found the two critical points $z_{\pm} = (\frac{1 \pm \sqrt{5}}{2})^5$, with respective thermal exponents $\alpha_- = 7/6$ and $\alpha_+ = 1/3$ governing the singularities of the thermodynamic free energy $f|_{sing} \sim |z - z_i|^{2-\alpha_i}$, $i = \pm$. These correspond respectively to the minimal CFT’s with $(p, q) = (2, 5)$ and $(p, q) = (5, 6)$ respectively, namely with central charge $c(2, 5) = -22/5$ and $c(5, 6) = 4/5$. These are the universality classes of the 2D Yang-lee edge singularity [13] and of the 2D critical three-state Potts model (a generalization of the Ising model with three spins instead of two).

As to the two other cases of hard squares and triangles, no exact solution is known to this day. The powerful Corner Transfer Matrix method of Baxter has allowed for many exact series expansions for thermodynamic quantities up to quite large orders [10] [11] eventually leading to the very reasonable conjecture that in these two bipartite cases the crystallization transition point lies in the universality class of the critical Ising model, at some critical value z_+ depending on the lattice, while the other critical point still lies in the Yang-Lee edge singularity class, at some z_- also depending on the lattice.

Beyond numerical evidence accumulated so far, we will propose here a “gravitational” proof of the identification of these universality classes via their random lattice version.

3.2. Matrix models as combinatorial tools

Matrix models are remarkably efficient tools to realize the summation over (possibly decorated) tessellations of given genus of the type of (2.5) (see e.g. [14] and [15] for reviews). The basic idea is to replace the task of performing say a Gaussian integration over an $N \times N$ Hermitian matrix M by the drawing of pictures, called “Feynmann diagrams”, weighted accordingly in such a way that the weighted sum over diagrams equals the Gaussian integral.

As an archetypical example of such a thing, let us display the quartic one-matrix model, with partition function

$$Z(g) = \int dM e^{-N \text{Tr}(\frac{M^2}{2} - g \frac{M^4}{4})} \quad (3.1)$$

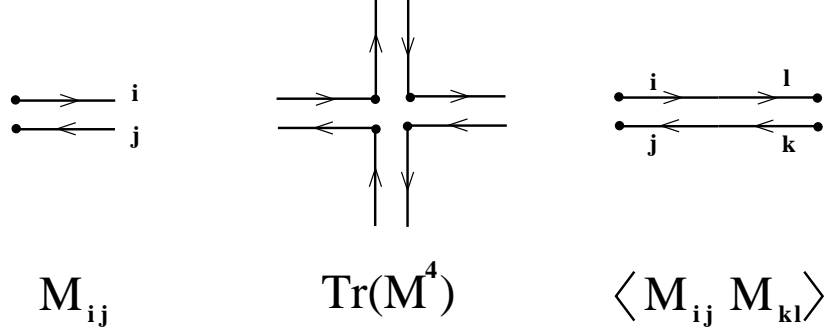


Fig. 3: The pictorial representation for matrix elements M_{ij} (double half-edges carrying matrix indices), terms $\text{Tr}(M^4)$ (a collection of four double half-edges connected at a vertex, with matrix indices conserved along the oriented lines), and the propagators used to glue pairs of double half-edges into edges in the fatgraphs representing the matrix integral.

where dM stands for the standard Haar measure, normalized in such a way that $Z(g = 0) = 1$. $Z(g)$ is to be understood as a formal power series of g , the coefficients of which must be computed by performing Gaussian matrix integrals. By virtue of Wick's theorem, this is readily done (for the coefficient Z_n of g^n) by computing

$$\begin{aligned}
Z_n &= \int dM e^{-N \text{Tr}(\frac{M^2}{2})} \frac{N^n}{n!} \text{Tr}\left(\frac{M^4}{4}\right)^n \\
&= \frac{(N/4)^n}{n!} \sum_{\text{pairs } (ij), (kl)} \prod_{ij, kl} \langle M_{ij} M_{kl} \rangle
\end{aligned} \tag{3.2}$$

where the sum extends over all decompositions of the matrix elements into pairs and the notation $\langle M_{ij} M_{kl} \rangle = \frac{1}{N} \delta_{il} \delta_{jk}$ stands for the “propagators” $\int dM e^{-N \text{Tr}(M^2/2)} M_{ij} M_{kl}$. In turn, the value of the propagator allows to devise a pictorial representation for the sum in (3.2). Representing a matrix element M_{ij} by a double half-edge as in Fig. 3, where each oriented line carries a matrix index running from 1 to N , we may express $\text{Tr}(M^4)$ as in Fig. 3, and interpret the sum in (3.2) as that over all possibly disconnected fatgraphs obtained by gluing half-edges into edges (propagators). Each such graph receives a weight $1/N$ per edge (from the propagators), Ng per vertex, and N per remaining oriented loop carrying an index summed from 1 to N . This gives an overall weight $g^A N^{F-E+A}$ for each possibly disconnected graph ($A = \#\text{vertices}$, $F = \#\text{faces}$ and $E = \#\text{edges}$), as well as an overall rational factor expressed as $\sum 1/(4^n n!)$, which is nothing but the inverse of the order of the automorphism group of the corresponding fatgraph. Finally upon taking the logarithm of $Z(g)$, one ends up with the desired sum over *connected* tessellations Θ (made

of squares here, dual to the tetravalent vertices of the matrix model), and with a weight $N^{\chi(\Theta)} g^{A(\Theta)} / |Aut(\Theta)|$. This particular example therefore corresponds to pure gravity, in the form of random quadrangulations. Note that the size N of the matrix serves as Newton constant in this approach, while the cosmological constant g is a feature of the potential (term in the non-gaussian part of the exponential weight).

More generally, we may engineer matrix models to suit our needs, either by considering a more general potential allowing for weighted vertices of arbitrary valencies, or/and by considering multi-matrix integrals of the form

$$Z = \int dA_1 \dots dA_k e^{-N \text{Tr}(\frac{1}{2} \vec{A}^t Q \vec{A} - \sum_{i=1}^k V_i(A_i))} \quad (3.3)$$

where \vec{A} denotes the column vector of matrices $(A_1, \dots, A_k)^t$ and Q is a $k \times k$ quadratic form (with $\vec{A}^t Q \vec{A} = \sum_{1 \leq a, b \leq k} Q_{ab} A_a A_b$), and the V_i some polynomial potentials. Note that again we normalize the measure in such a way that $Z = 1$ if the V_i vanish. The diagrammatic interpretation of Z follows from the multi-matrix generalization of Wick's theorem expressing the multi-Gaussian matrix integral as a sum over pair decompositions of matrix elements of the integrand evaluated by using propagators, namely

$$\langle f(\{(A_a)_{ij}\}) \rangle_Q = \sum_{\text{pairings}} \prod_{\text{pairs}} \langle (A_a)_{ij} (A_b)_{kl} \rangle_Q \quad (3.4)$$

where $\langle \dots \rangle_Q = \int \prod_a dA_a \dots e^{-N \text{Tr}(\frac{1}{2} \vec{A}^t Q \vec{A})}$ stands for the multi-Gaussian average. In particular, propagators are easily computed in terms of the *inverse* of the quadratic form Q :

$$\langle (A_a)_{ij} (A_b)_{kl} \rangle_Q = \frac{\delta_{il} \delta_{jk}}{N} (Q^{-1})_{a,b} \quad (3.5)$$

The diagrammatic interpretation of Z is now clear: attach different “colors” $a = 1, 2, \dots, k$ to the matrices. The potentials $V_i(x) = \sum g_{i,m} x^m / m$ contain the list of allowed vertices of color i and valence m with their respective weights $g_{i,m}$. The quadratic form Q encodes via its inverse the allowed propagators, namely the list of possible edges linking these vertices to one another. The result is a sum over vertex-colored graphs with specific gluing rules. Note moreover that irrespectively of its color each vertex receives a weight N , each edge a weight $1/N$ and each loop of oriented index lines a factor N , which still produces the topological factor N^χ in the expansion of $\text{Log } Z$, χ the Euler characteristic of the (decorated) connected graph. This allows in particular to extract the contribution from planar graphs by taking $N \rightarrow \infty$.

In the next two sections, we use some of these models to solve the hard-particle problem on various random lattices.

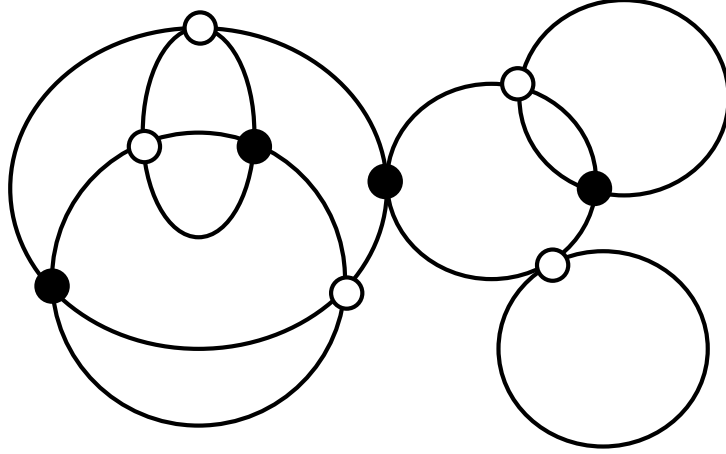


Fig. 4: A typical configuration of hard particles on a tetravalent planar graph. The particles are represented by filled circles (\bullet). They obey the nearest neighbor exclusion constraint that no two particles may be adjacent to the same edge.

3.3. Hard objects on random tetravalent graphs: matrix model solution

We now turn to the enumeration of hard-particle configurations on random tetravalent graphs, the natural fluctuating versions of the square lattice. For illustration we display in Fig. 4 a typical hard-particle configuration on a connected planar tetravalent graph. The occupied vertices (represented by filled circles) obey the nearest-neighbor exclusion (hardness) constraint that no two particles may be adjacent to the same edge. As explained before, we attach a weight z per particle and g per vertex.

In view of previous section, we are now ready to write a *two-matrix* model for enumerating such configurations, with partition function

$$Z(g, z) = \int dA dB e^{-N \text{Tr}(AB - \frac{A^2}{2} - gz \frac{A^4}{4} - g \frac{B^4}{4})} \quad (3.6)$$

where the measure is now normalized in such a way that $Z(g = 0, z) = 1$. The graphical interpretation (see Fig. 5) is a consequence of the two-matrix form of the Wick theorem, in which propagators are calculated using the Gaussian weight $e^{-N \text{Tr}(AB - A^2/2)}$, namely with $\langle A_{ij} B_{kl} \rangle = \delta_{il} \delta_{jk} / N$ and $\langle B_{ij} B_{kl} \rangle = \delta_{il} \delta_{jk} / N$ while $\langle A_{ij} A_{kl} \rangle = 0$ as a particular case of eqn. (3.5). Representing the terms $\text{Tr}(B^4)$ as empty tetravalent vertices and $\text{Tr}(A^4)$ as occupied ones, we see that the gluing of half-edges into edges (through the propagators) now incorporates the hard-particle exclusion rule that no two occupied vertices may be adjacent (vanishing of the $\langle AA \rangle$ propagator). Again, $\text{Log } Z(g, z)$ is the generating function

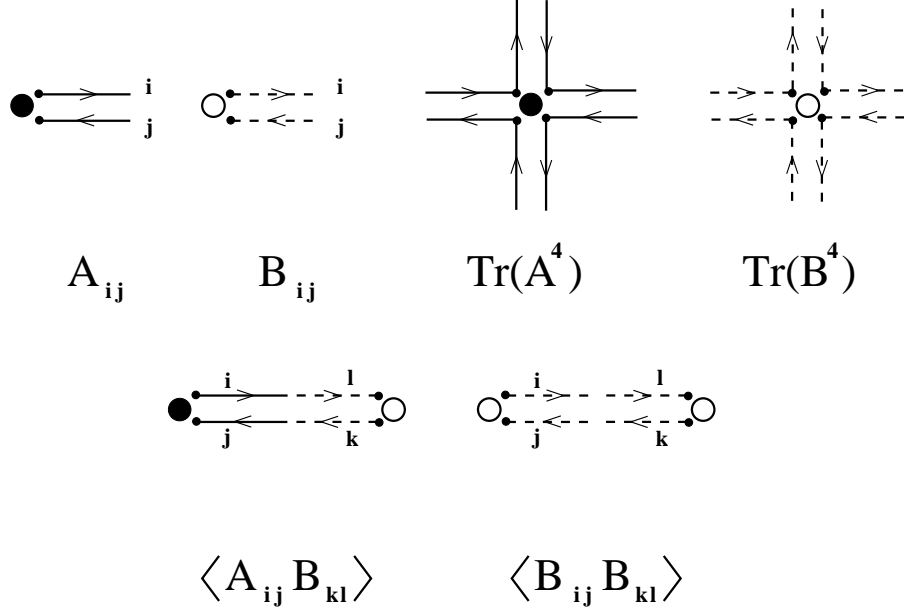


Fig. 5: The pictorial representation for the matrix elements of the two-matrix model describing hard-particles on tetravalent fatgraphs. The occupied (resp. empty) vertices correspond to the confluence of four A (resp. B) matrix elements, represented as solid (resp. dashed) double half-lines. We have also represented the only two non-vanishing propagators allowing for gluing double half-edges into edges of the final graph. These obey the particle exclusion rule that no two adjacent vertices of the final graph may be simultaneously occupied. This information is encoded in the quadratic piece of the potential of the two-matrix model.

for connected fatgraphs with hard particles on them, and with a weight g per vertex, z per occupied vertex, times $N^{\chi(\Gamma)}/|Aut(\Gamma)|$ for the decorated graph Γ .

The calculation of the matrix integral (3.6) goes through a succession of standard steps.

- **Step 1** consists in replacing the integral by one over eigenvalues of the matrices, using the Itzykson-Zuber formula [16]. One is left with

$$Z(g, z) = \int d^N a d^N b \Delta(a) \Delta(b) e^{-N \text{Tr}(ab - \frac{a^2}{2} - gz \frac{a^4}{4} - g \frac{b^4}{4})} \quad (3.7)$$

where a and b are real diagonal matrices of size $N \times N$, and Δ stands for the Vandermonde determinant $\Delta(a) = \det[a_i^{j-1}]_{1 \leq i, j \leq N}$.

- **Step 2** consists in first noting that $\Delta(a) = \det[p_{j-1}(a_i)]_{1 \leq i, j \leq N}$, for any sequence of monic polynomials p_j of degree j . One then picks the two sets p_j and q_m to be inserted in $\Delta(a)$ and $\Delta(b)$ respectively in such a way that they form a bi-orthogonal set wrt the

following bilinear form:

$$(f, g) = \int dx dy e^{-N(xy - x^2/2 - gzx^4/4 - gy^4/4)} f(x)g(y) \quad (3.8)$$

formally defined by using the size-one matrix propagators. Writing

$$(p_j, q_m) = \delta_{j,m} h_j(g, z) \quad (3.9)$$

one then computes

$$Z(g, z) = \prod_{i=0}^{N-1} \frac{h_i(g, z)}{h_i(0, z)} \quad (3.10)$$

• **Step 3** consists in calculating the h_j 's. One introduces the operators Q_1 and Q_2 of multiplication by x and y , expressed respectively on the basis $p_j(x)$ and $q_m(y)$. Introducing similarly $P_1 = d/dx$ and $P_2 = d/dy$, one obtains upon integration by parts the following relations

$$\begin{aligned} \frac{P_1}{N} &= Q_2^\dagger - Q_1 - gzQ_1^3 \\ \frac{P_2}{N} &= Q_1^\dagger - gQ_2^3 \end{aligned} \quad (3.11)$$

where the adjoint is obtained by letting the corresponding operator act on the other polynomial basis. As a consequence of (3.11), the Q operators take the form

$$\begin{aligned} Q_1 p_n(x) &= p_{n+1}(x) + r_n p_{n-1}(x) + s_n p_{n-3}(x) \\ Q_2 q_m(y) &= q_{m+1}(y) + \tilde{r}_m q_{m-1}(y) + \tilde{s}_m q_{m-3}(y) \end{aligned} \quad (3.12)$$

Note the presence of only every other term, due to the \mathbb{Z}_2 symmetry of the potential under $A \rightarrow -A, B \rightarrow -B$. The fact that Q_1 and Q_2 have a finite range is generic in multimatrix models with polynomial potentials. The equations (3.11) finally turn into recursion relations for the various coefficients of (3.12), which upon elimination allow for expressing $v_n = h_n/h_{n-1}$, and finally the free energy

$$F(g, z) = \frac{1}{N^2} \text{Log } Z(g, z) = \frac{1}{N^2} \sum_{i=0}^N (N-i) \text{Log} \left(\frac{v_i(g, z)}{v_i(0, z)} \right) \quad (3.13)$$

• As we will be only interested in the large N limit, in which only planar graphs are selected (with genus zero free energy $f_0(g, z) = \lim_{N \rightarrow \infty} F(g, z)$), let us perform the **Step 4**, namely the reduction of equations in the large N case. We make the standard assumption that all coefficients r_n, h_n , etc... tend to smooth functions of $x = n/N$ for

$n, N \rightarrow \infty$ while x remains fixed. This is certainly true in the vicinity of the Gaussian model, for small g . We have the limits

$$v_n \rightarrow v(x), \quad r_n \rightarrow r(x), \quad s_n \rightarrow s(x) \quad (3.14)$$

and similarly for the tilded quantities. In the same limit, the Q operators (3.12) become simply

$$\begin{aligned} Q_1 &\rightarrow \sigma + r\sigma^{-1} + s\sigma^{-3} \\ Q_2 &\rightarrow \tau + \tilde{r}\tau^{-1} + \tilde{s}\tau^{-3} \end{aligned} \quad (3.15)$$

where the commuting dummy variables σ, τ are inherited from the corresponding (non-commuting) index shift operator acting on the respective polynomial bases. In particular, the operator adjoint simply follows from $\tau^\dagger = v\sigma^{-1}$. Plugging (3.15) into (3.11) and noting that $P_1/N = x\sigma^{-1} + O(\sigma^{-2})$, we finally get a set of algebraic equations for the r 's and s 's as well as their tilded counterparts. Defining rescaled versions $V = gv$, $R = gr$, $S = g^2s$ and similarly for the tilded quantities, we get

$$\begin{aligned} gx &= V - R - 3z(R^2 + S) \\ 0 &= \tilde{R} - V(1 + 3zR) \\ 0 &= \tilde{S} - zV^3 \\ 0 &= R - 3V\tilde{R} \\ 0 &= S - V^3 \end{aligned} \quad (3.16)$$

These algebraic equations were given a combinatorial interpretation in [17] [18], where the various functions V, R, S, \dots were shown to generate decorated rooted trees. After elimination, the system (3.16) reduces to

$$gx = \varphi(V) \equiv V(1 - 3zV^2) - \frac{3V^2}{(1 - 9zV^2)^2} \quad (3.17)$$

For fixed g and z this equation defines upon inversion the unique function $V(x)$ such that $V(x) = gx + O(g^2)$ at small g . It encodes the asymptotic properties of the sequence v_n , hence those of the h_n 's, and finally we have

$$f_0(g, z) = \int_0^1 dx (1-x) \text{Log} \left(\frac{V(x)}{gx} \right) \quad (3.18)$$

where we have identified $v(0, z) = x$.

It is now a simple exercise to find the singularities of the thermodynamic function $f_0(g, z)$. Noting indeed that

$$\frac{d^2}{dg^2} g^3 \frac{d}{dg} f_0(g, z) = \frac{gd}{dg} \text{Log} \left(\frac{V_{g,z}}{g} \right) \quad (3.19)$$

where $V_{g,z}$ is simply the unique solution to $g = \varphi(V_{g,z})$ such that $V_{g,z} = g + O(g^2)$ (identical to $V(x=1)$), we see that the singularities of the free energy are those of $V_{g,z}$. Defining the critical cosmological constant by

$$\begin{aligned} g_c(z) &= \varphi(V_c(z)) \\ 0 &= \varphi'(V_c(z)) \end{aligned} \quad (3.20)$$

where $V_c(z)$ is the smallest value of V where a maximum of φ is attained, we immediately get the critical behavior $f_0|_{\text{sing}} \sim (g_c(z) - g)^{2-\gamma}$ where $\gamma = -1/2$, as this generically corresponds to a square root singularity of V from $(g - g_c) \sim \varphi''(V_c)(V - V_c)^2/2$. Eqns. (3.20) are easily parametrized as

$$z = \frac{12u(1+3u)^2}{(1-3u)^8} \quad g_c(z) = \frac{(1-3u)^4(1+10u-15u^2)}{12(1+3u)^2} \quad (3.21)$$

This gives a critical curve ending at the point

$$\begin{aligned} z_- &= -\frac{25}{8192}(11\sqrt{5} + 25) < 0 \\ g_- &= g_c(z_-) = \frac{64}{45}(13\sqrt{5} - 29) \\ V_- &= V_c(z_-) = \frac{32}{75}(7\sqrt{5} - 15) \end{aligned} \quad (3.22)$$

and where in addition we have $\varphi''(V_-) = 0$, which implies a susceptibility exponent $\gamma = -1/3$, as we now have an equation of the form $g - g_- \sim \varphi'''(V_-)(V - V_-)^3/6$.

To conclude, we find only one critical value of z at a negative value z_- , corresponding to a non-unitary critical point. The value $\gamma = -1/3$ can be carefully traced back to the coupling of the Yang-Lee edge singularity with $c(2, 5) = -22/5$ to 2DQG³. This shows

³ This is in apparent contradiction with the formula (2.7) which would lead to $\gamma_{str} = -3/2$. This is due to the fact that the leading behavior observed in the matrix model solution corresponds to another *scale* set not by the identity operator (leading by integration over the random surfaces to the area $A = \int I dd^2 z$ or to the conjugated coupling g via the off-critical term $(g_c - g) \int I dd^2 z$

that no crystallization transition takes place when we couple the hard-particle model to ordinary 2DQG.

Let us however complete the task of computing the free energy. Using the Lagrange inversion formula, we may explicitly invert (3.17) and evaluate any function of $V_{g,z}$:

$$h(V_{g,z}) = \sum_{n \geq 1} \frac{g^n}{n} \oint \frac{dw}{2i\pi} \frac{h'(w)}{\varphi(w)^n} \quad (3.23)$$

Expressing $f_0(g, z) = \sum_{n \geq 1} f_n(z) g^n$, and using eqn. (3.19), we find that $f_n(z) = \varphi_n(z)/((n+1)(n+2))$, where $\varphi_n(z)$ are generated by $\text{Log}(V_{g,z}/g) = \sum_{n \geq 1} \varphi_n(z) g^n$. We may now use the Lagrange inversion formula (3.23) for $h(V) = \text{Log}(V)$. This gives

$$\varphi_n(z) = \frac{1}{n} \oint \frac{dw}{2i\pi w} \frac{1}{\varphi(w)^n} \quad (3.24)$$

This finally leads to the compact formula for the free energy $f_n(z)$ for hard particles on planar tetravalent fatgraphs with n vertices, and a weight z per particle:

$$\begin{aligned} f_n(z) &= \frac{1}{n(n+1)(n+2)} \sum_{\substack{l, p \geq 0 \\ 2(l+p) \leq n}} \binom{2n-2l-2p-1}{n-1} \times \\ &\times \binom{2n-l-2p-1}{l} \binom{4n-2l-p-2}{p} 3^{n-l} z^{l+p} \end{aligned} \quad (3.25)$$

As a side remark, we recover the result for pure tetravalent graphs when $z = 0$, namely $f_n(z = 0) = 3^n \binom{2n}{n} / (2n(n+1)(n+2)) = N_n/n$, N_n as in (2.12) (the discrepancy is due to the extra rooting in (2.12) which implies $N_n = n f_n$). More interestingly, if we take $z \rightarrow \infty$

in the gravitational action) but by that with the lowest (negative) conformal dimension, as is the case in all non-unitary theories with $c(p, q)$, say with $q > p + 1$. This operator has conformal dimension $h_0 = (1 - (p - q)^2)/(4pq)$, and gravitationally dressed dimension $\Delta_0 = (p - q + 1)/(2p)$ from (2.8). It corresponds to a term $(\mu_c - \mu) \int \Phi_{h_0} d^2 z$ in the gravitational action, where by a dimensional argument we find $g_c - g \sim (\mu_c - \mu)^{1-\Delta_0}$. The exponent γ observed in the matrix model corresponds to the scaling in terms of $\mu_c - \mu$. Once translated back into the language of the correct cosmological constant $g_c - g$, we have $f|_{\text{sing}} \sim (\mu_c - \mu)^{2-\gamma} \sim (g_c - g)^{\frac{2-\gamma}{1-\Delta_0}} = (g_c - g)^{2-\gamma_{str}}$. This allows to finally identify $\gamma = -2/(p + q - 1)$ for any minimal model, while $\gamma_{str} = (p - q)/p$ follows from (2.7). Here, for $\gamma = -1/3$ we must have $p + q = 7$, hence $p = 2, q = 5$. The only other possibility would be $p = 3$ and $q = 4$, but the corresponding model is unitary and could not have a negative critical value of z as in (3.22).

in (3.25), we should tend to a crystalline groundstate in which vertices of the graphs are maximally occupied. We find that only f_{2n} survive, with the result

$$f_{2n} = \frac{3^{n-1}}{n(2n+1)(2n+2)} \binom{3n}{n} \quad (3.26)$$

The number $(2n)f_{2n}$ counts the rooted bipartite tetravalent planar graphs [19] [20]. Another way of understanding this result, is by looking directly at the matrix integral (3.6). Indeed, performing the change of matrix variables $A \rightarrow A/z^{\frac{1}{8}}$, $B \rightarrow Bz^{\frac{1}{8}}$ and redefining $g \rightarrow g/\sqrt{z}$, we immediately see that in the limit $z \rightarrow \infty$ the matrix integral (3.6) reduces to

$$Z(g, \infty) = \int dA dB e^{-N \text{Tr}(AB - \frac{g}{4}(A^4 + B^4))} \quad (3.27)$$

which clearly enumerates the bipartite tetravalent graphs.

The lesson to be drawn from this section is that summing over *arbitrary* tetravalent graphs destroys the crystallization transition of the hard-particle model. However, the crystalline groundstates which would make this transition possible dominate the sum at large z , and involve only *bipartite* tetravalent graphs. The problem is that these graphs have a negligible contribution at all finite values of z . This suggests to reduce the range of summation to bipartite graphs from the very beginning, which is the subject of next section.

3.4. Hard objects on bipartite trivalent graphs: matrix model solution

Simply for pedagogical purposes, we will address here the problem of enumeration of hard-particle configurations on *trivalent bipartite* fatgraphs. The case of tetravalent graphs was solved in [1], and presents only technical complications, whereas the final results concerning the crystallization transition and its universality class are the same. So we choose to concentrate here on the case of hard-triangles coupled to 2DQG.

We wish to generate bipartite trivalent graphs say with alternating black and white vertices, which in addition may be either occupied or empty. To generate the desired decorated graphs, we now need four matrices A_1, A_2, A_3, A_4 each standing for half-edges connected to empty white, occupied black, occupied white and empty black vertices. The corresponding matrix integral reads

$$Z(g, z) = \int dA_1 dA_2 dA_3 dA_4 e^{-N \text{Tr} V(A_1, A_2, A_3, A_4)} \quad (3.28)$$

$$V(A_1, A_2, A_3, A_4) = A_1 A_2 - A_2 A_3 + A_3 A_4 - g \left(\frac{A_1^3}{3} + \frac{A_4^3}{3} \right) - gz \left(\frac{A_2^3}{3} + \frac{A_3^3}{3} \right)$$

The quadratic form in $V(A_1, A_2, A_3, A_4)$ has been engineered so as to reproduce the correct propagators, namely that only black and white vertices are connected in the Feynman diagrams ($\langle A_i A_j \rangle = 0$ if i and j have the same parity) and that two occupied vertices exclude one-another ($\langle A_2 A_3 \rangle = 0$).

We may now repeat the straightforward, though tedious, steps 1-4 of the previous section.

- **Step 1** takes us to the eigenvalue integral

$$Z(g, z) = \int d^N a_1 d^N a_2 d^N a_3 d^N a_4 \Delta(a_1) \Delta(a_4) e^{-N \text{Tr } V(a_1, a_2, a_3, a_4)} \quad (3.29)$$

where the a_i are real diagonal matrices of size $N \times N$.

- **Step 2** goes through as well, by simply replacing the bilinear form (3.8) by

$$(f, g) = \int dx_1 dx_2 dx_3 dx_4 e^{-NV(x_1, x_2, x_3, x_4)} f(x_1) g(x_4) \quad (3.30)$$

• **Step 3:** we define analogously operators Q_i, P_i , $i = 1, 2, 3, 4$, acting on the left orthogonal polynomial basis for $i = 1, 2$ and on the right for $i = 3, 4$, and satisfying the following system, obtained by integration by parts:

$$\begin{aligned} \frac{P_1}{N} &= \partial_{x_1} V(Q_1, Q_2, Q_3, Q_4) = Q_2 - gQ_1^2 \\ \frac{P_2}{N} &= 0 = \partial_{x_2} V(Q_1, Q_2, Q_3, Q_4) = Q_1 - Q_3 - gzQ_2^2 \\ \frac{P_3}{N} &= 0 = \partial_{x_3} V(Q_1, Q_2, Q_3, Q_4) = Q_4 - Q_2 - gzQ_3^2 \\ \frac{P_4}{N} &= \partial_{x_4} V(Q_1, Q_2, Q_3, Q_4) = Q_3 - gQ_4^2 \end{aligned} \quad (3.31)$$

The obvious symmetry of the potential under the interchange $x_i \leftrightarrow x_{5-i}$ allows to infer that $Q_4 = Q_1^\dagger$ and $Q_3 = Q_2^\dagger$, so that the main equations reduce simply to

$$\begin{aligned} \frac{P_1}{N} &= Q_2 - gQ_1^2 \\ Q_1 &= Q_2^\dagger + gzQ_2^2 \end{aligned} \quad (3.32)$$

The corresponding Q -operators are easily expressed on the left basis of orthogonal polynomials as

$$\begin{aligned} Q_1 &= \sigma + \sigma^{-2} r^{(1)} + \sigma^{-5} r^{(2)} + \sigma^{-8} r^{(3)} \\ Q_2 &= \sigma^2 s^{(0)} + \sigma^{-1} s^{(1)} + \sigma^{-4} s^{(2)} \end{aligned} \quad (3.33)$$

where σ is the shift operator acting on the p 's as $\sigma p_n = p_{n+1}$ and the operators $r^{(i)}, s^{(i)}$ are diagonal. The presence of only powers of σ spaced by multiples of 3 is a consequence of the accidental \mathbb{Z}_3 -symmetry of the potential V , namely that $V(\omega x_1, \bar{\omega} x_2, \omega x_3, \bar{\omega} x_4) = V(x_1, x_2, x_3, x_4)$ for $\omega = e^{\frac{2i\pi}{3}}$. The equations (3.32) together with the fact that $P_1/N \sim (n/N)\sigma^{-1} + O(\sigma^{-2})$ allow in principle for solving the model for all N by expressing recursion relations for the quantity $v_n = h_n/h_{n-1}$.

• **Step 4:** We are however only interested here in the planar $N \rightarrow \infty$ limit, in which σ becomes a commuting dummy variable, and the $r^{(i)}, s^{(i)}$ some functions of $x = n/N$, while $n, N \rightarrow \infty$. The equations (3.32) translate simply into algebraic equations for these functions, as well as for $v(x) = \lim v_n$. Upon defining the rescaled quantities $R^{(1)} = g^3 z^2 r^{(1)}$, $S^{(0)} = s^{(0)}/g$, $S^{(1)} = g^2 z s^{(1)}$, $S^{(2)} = g^5 z^2 s^{(2)}$ and $V = g^2 z v$, we find the algebraic system

$$\begin{aligned} S^{(0)} &= 1 \\ S^{(2)} &= -zV^4 \\ V &= S^{(1)} + 2S^{(1)}V \\ R^{(1)} &= V^2 + z(S^{(1)})^2 + 2zS^{(2)} \\ g^2 z^2 x &= zS^{(1)} - 2R^{(1)} \end{aligned} \tag{3.34}$$

By elimination, we are simply left with

$$g^2 z^2 x = \varphi(V) \equiv z \frac{V}{(1+2V)^2} - 2V^2(1-2V^2) \tag{3.35}$$

while the desired planar free energy reads $f_0(g, z) = \int_0^1 (1-x) \text{Log}(V/(g^2 z x))$ by virtue of the obvious generalization of (3.18). The function V must be computed by inverting (3.35) order by order in $g^2 x$. As in the case of previous section, the singularities of the planar free energy come from those of the solution $V_{g,z}$ of (3.35) at $x = 1$, as we still have a relation of the form $d^2/dg^2 g^3 d/dg f_0(g, z) = g d/dg \text{Log}(V_{g,z}/(g^2 z))$.

Expressing the critical points $g_c(z)$ solving the obvious adaptation of (3.20), namely that $g_c(z)^2 = \varphi(V_c(z))/z^2$, while $\varphi'(V_c(z)) = 0$, with the appropriate value of φ from (3.35), we see a first difference with the case of previous section, namely that as

$$\varphi'(V) \sim (1-2V)(z-4V(1+2V)^4) \tag{3.36}$$

we now have *two* critical curves

$$\begin{aligned} g_1^2(z) &= \frac{1}{8z} - \frac{1}{4z^2}, \quad z > 0, \quad V = 1/2 \\ g_2^2(z) &= \frac{1+8V+10V^2}{8(1+2V)^8}, \quad \text{with } z(V) = 4V(1+2V)^4 \end{aligned} \tag{3.37}$$

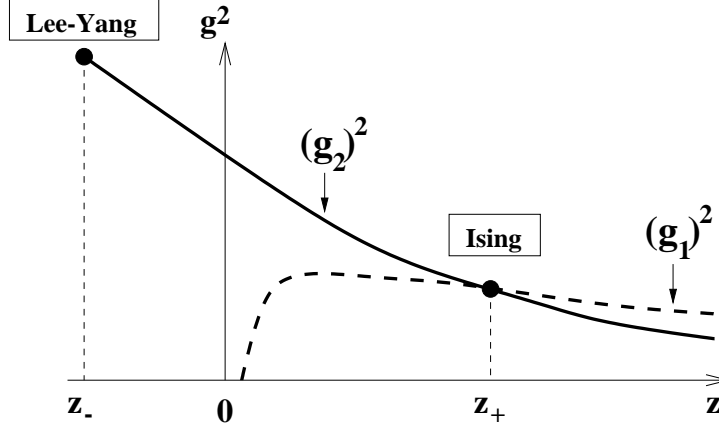


Fig. 6: The critical curves $g_c^2(z)$ are represented in solid (g_2^2) and dashed (g_1^2) lines. The higher critical endpoint $z_- = -2^9/5^5$ and intersection point $z_+ = 32$ respectively correspond to the Yang-Lee edge singularity and to the critical Ising model both coupled to 2DQG.

along which we generically have a string susceptibility exponent of $\gamma = -1/2$. These are displayed in Fig. 6. While the curve $g_2^2(z)$ possesses an endpoint at a value $z = z_- = -2^9/5^5$ (where $V_- = -1/10$, and $g_-^2 = 3.5^7/2^{20}$) at which φ'' vanishes and which qualitatively resembles that found in the previous section, we now get another critical point at the intersection of the two curves $g_1^2(z)$ and $g_2^2(z)$ at $z = z_+ = 2^5$ (with $V_+ = 1/2$ and $g_+^2 = 15/2^{12}$) where we also have a vanishing of φ'' . Both critical points correspond to $\gamma = -1/3$, but while the first one is at a negative value of z (hence expected to be described by a non-unitary CFT), the other one is at a positive value of z . The only two minimal model candidate CFT's for $\gamma = -1/3$ are such that $p + q = 7$ (from the relation $\gamma = -2/(p + q - 1)$). This leaves us with only the Yang-Lee edge singularity, non-unitary with $c(2, 5) = -22/5$, and the critical Ising model, unitary with $c(3, 4) = 1/2$. Noting that the second critical point found separates two phases of low and high occupancy, we deduce from the above discussion that the endpoint corresponds to the Yang-Lee model coupled to 2DQG, while the intersection point corresponds to the crystallization transition, and is described by the critical Ising model coupled to 2DQG. This assertion is further confirmed by actually computing critical exponents corresponding to various operators (see [1] for details). This completes our gravitational proof that the hard triangle model's crystallization transition lies in the universality class of the critical Ising model.

Let us for completeness express the planar free energy's coefficients $f_{2n}(z)$ of g^{2n} in the (even) g -expansion, by inverting (3.35) via the Lagrange inversion formula. Repeating

the arguments of the previous section, we arrive at

$$f_{2n}(z) = \frac{2^n}{n(n+1)(n+2)} \sum_{0 \leq 2p \leq j \leq n} \left(-\frac{1}{2}\right)^p \binom{2n-j-1}{n-1} \binom{n-j}{p} \binom{4n-2j}{j-2p} z^j \quad (3.38)$$

Note this time the presence of signs in the polynomial expression for $f_{2n}(z)$. Note also that for $z = 0$ we recover the number of bipartite trivalent planar graphs with $2n$ vertices $N_{2n} = 2nf_{2n}(z=0) = 2^{n-1} \binom{2n}{n} / ((n+1)(n+2))$ dual to the number of Eulerian triangulations of area $2n$ [19] [20]. The above results also translate into large n asymptotics of $f_{2n}(z)$ via (2.10), namely that

$$\begin{aligned} f_{2n}(z) &\sim \frac{g_c(z)^{-2n}}{n^{\frac{7}{2}}} && \text{with } \begin{cases} g_c(z) = g_2(z) & z_- < z < z_+ \\ g_c(z) = g_1(z) & z > z_+ \end{cases} \\ f_{2n}(z_{\pm}) &\sim \frac{g_c(z_{\pm})^{-2n}}{n^{\frac{10}{3}}} && \text{with } \begin{cases} g_c(z_-) = \sqrt{15} \cdot \frac{5^3}{2^{10}} \\ g_c(z_+) = \frac{\sqrt{15}}{2^6} \end{cases} \end{aligned} \quad (3.39)$$

3.5. Partial conclusion

Using matrix model techniques, we have been able to observe how geometrical constraints (on the hard-particle models) have made bipartiteness of the random lattices relevant. Indeed, imposing bipartiteness of the underlying graphs from the very beginning proves to be instrumental in restoring the expected crystallization transition. This allows to give a formal gravitational proof in the cases of hard triangles (as well as hard squares) that this transition is indeed in the universality class of the 2D critical Ising model. Some generalizations of the models shown here have been worked out in [1] and concern particle models subject to a weaker exclusion constraint. These allow in principle to visit all critical points described by minimal models coupled to 2DQG, and must all be defined on bipartite graphs as well.

One could wonder what happens in the case of hard hexagons. Inspired by the previous lesson, we would expect that the crystallization transition for hard hexagons only survives on *tripartite* (i.e. vertex-tricolored) fatgraphs. We expect indeed the existence of three symmetric competing maximally occupied crystalline groundstates to induce a transition in the universality class of the critical 3 state Potts model coupled to 2DQG. Attempts in this direction show that a certain rectangular matrix model should do the job of generating the corresponding configurations of hard particles on tricolored trivalent graphs, but this model has not been amenable to an exact solution yet [22].

As a both final and preliminary remark for the remainder of this note, the crucial properties of *colorability* of the random lattices we have summed over have guaranteed the existence of crystalline *groundstates*, also responsible for the existence of the phase transition. In the next example of meanders, we will also arrive at a similar discussion of critical properties according to the colorability constraints of the random lattices we will sum over. However in this new case, not only the structure of groundstates does rely on the colorability constraint, but the very definition of the degrees of freedom of the model as well, essential in determining the central charge of the underlying CFT.

4. Meanders

In this second part, we address the apparently unrelated problem of enumeration of meanders, namely of topologically inequivalent configurations of a road (simple closed curve) crossing a river (infinite line) through a given number $2n$ of bridges (simple intersections). After first describing the problem in detail, we will turn to a description of the meander configurations as some particular random tetravalent planar graphs decorated by loops (actually two loops: the road, and the river). This leads us naturally to study the more general problem of loop models coupled to 2DQG. In carefully pursuing this, we will eventually see that geometrical constraints on these models (the so-called fully-packed loop models) make again the *colorability* of the underlying lattice relevant, like in the hard-particle case. We will be able to identify the meander universality class by a subtle reasoning on the type of random lattices we must sum over to finally generate the correct meander configurations.

4.1. The meander enumeration problem

Meanders are defined as planar graph configurations of a closed nonselfintersecting curve (road) crossing a line (river) through a fixed number $2n$ of simple intersection points (bridges). These configurations must be counted up to smooth deformations preserving the topology. We denote by M_{2n} the total number of such distinct configurations for given number of bridges $2n$. The meander enumeration is an old problem: it can probably be traced back to some work by Poincaré (1911), and reemerged in various contexts since: as mathematical recreation [23], as folding problem [24] [25], in relation to the 16th Hilbert problem [26], in the theory of invariants of 3-manifolds [27], in computer science [28], in abstract algebraic terms [29] [30], and in its own right [31] [32] [33] [34].

In the works [25] and subsequent, our main motivation was the study of the folding problem of polymer chains. Such a polymer is ideally described by a chain of identical line segments attached by their ends, which serve as hinges between adjacent segments. Think of a single strip of stamps, which can be folded along the edges common to each neighboring stamps. We will distinguish between closed and open polymers according to whether the chain forms a loop or is open with two free ends. We will be addressing the *compact self-avoiding* folding of such objects, namely study the various ways in which the polymer can be completely folded onto one of its segments. Note that a closed compactly foldable polymer must have an even number of segments.

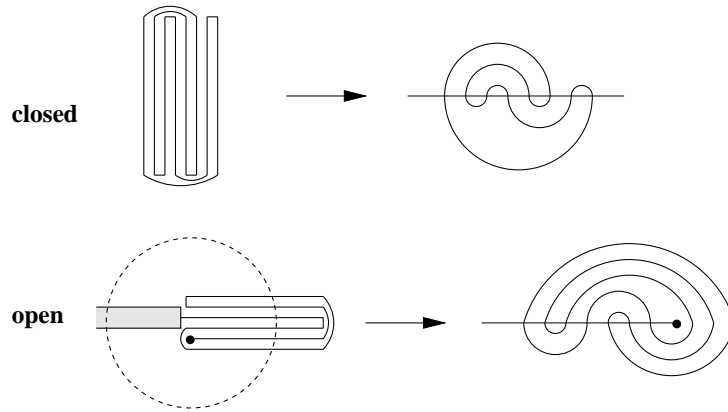


Fig. 7: Two compactly folded polymers and the corresponding meanders. The first example is a closed polymer with 8 segments, and corresponds to a meander with 8 bridges. The second example is an open polymer with 6 segments, and corresponds to a semi-meander with 7 bridges.

To distinguish between the various ways of compactly folding a closed polymer, we will represent the folded objects as a meander with $2n$ bridges. To visualize the relation between compactly folded closed polymers and meanders, it is simplest to imagine we draw a line perpendicular to the segments forming the folded polymer with a total of $2n$ intersections (each segment intersects the line once), and then separate the various segments (see Fig.7).

In the case of an open polymer with say $n - 1$ segments, let us attach one of its ends to say a wall or a support (see Fig.7), so as to prevent the polymer from winding around that end (this is exactly the situation in a strip of stamps, attached by one end to its support). Starting from a compactly folded configuration, let us again draw this time a circle that intersects each of the n segments once, and also intersects the support once. Extending the polymer so as to let it form a half-line with origin its free end, we form a

planar configuration of a non-selfintersecting loop (road) crossing a half-line (river with a source) through n points. These configurations considered up to smooth deformations preserving the topology are called *semi-meanders* (see Fig.7 for an illustration). The total number of semi-meanders with n bridges is denoted by \bar{M}_n .

The aim of the subsequent sections is to give a semi-rigorous physical argument leading to the prediction of the meander and semi-meander configuration exponents $\alpha, \bar{\alpha}$ which govern the large n asymptotics of the corresponding numbers $M_{2n} \sim g_c^{-2n}/n^\alpha$ and $\bar{M}_n \sim g_c^{-n}/n^{\bar{\alpha}}$, g_c some constant. This is done by identifying the universality class of the corresponding critical phenomenon, characteristic of the compact folding of one-dimensional objects. We try here to summarize and put in perspective various works among which the paper [2] where these results were first obtained.

4.2. Fixed lattice results for (fully-packed) loop models

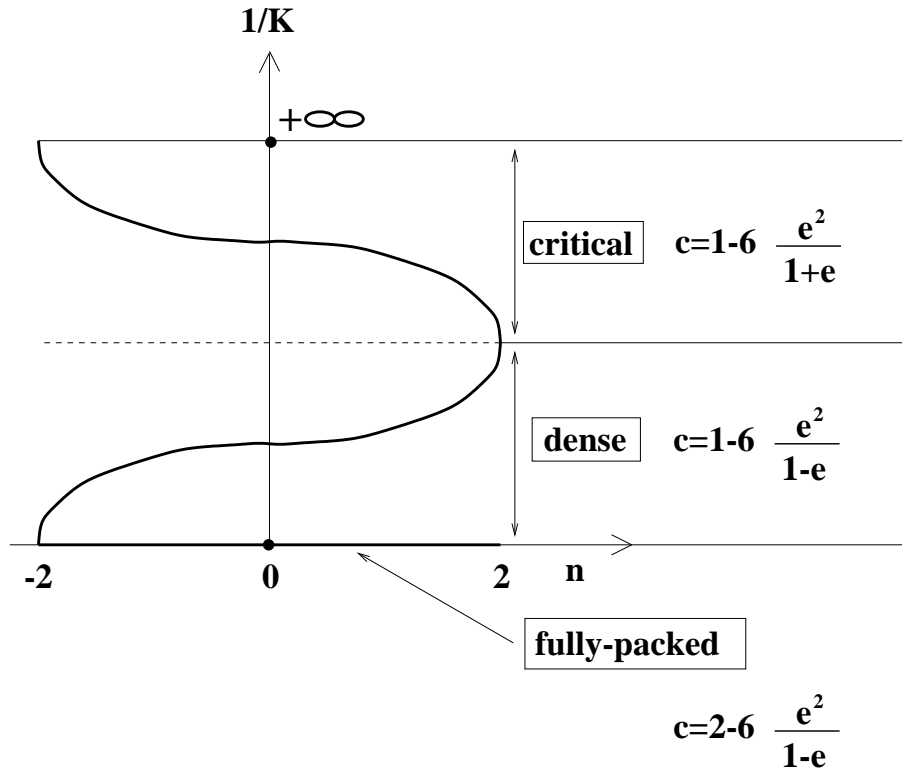


Fig. 8: Qualitative phase diagram of the $O(n)$ model on the honeycomb lattice. The thick lines correspond to critical curves, for which we have indicated the value of the central charge. We have parametrized $n = 2 \cos \pi e$, $0 \leq e \leq 1$.

Loop models have been studied extensively for decades as toy models for describing (self-avoiding) polymers and we will only summarize the results obtained for their critical behavior in two dimensions. They are defined as statistical lattice models, for which the configuration maps σ go from the set of edges of the lattice to $\mathcal{T} = \{0, 1\}$, where $\sigma(e) = 1$ iff the edge e is occupied by a loop edge.

More specifically let us first discuss the case of loop (so-called $O(n)$) models on the honeycomb lattice. The self-avoidance constraint is very easy to implement as at most one loop may visit any given vertex, hence at each vertex with adjacent edges e, e', e'' , we either have $\sigma(e) = \sigma(e') = \sigma(e'') = 0$, or exactly two of the edges are occupied say $\sigma(e) = \sigma(e') = 1$, while $\sigma(e'') = 0$. We attach two types of Boltzmann weights to the loop configurations: a weight K per occupied edge, and a weight n per loop. The partition function of the model reads

$$Z(n, K) = \sum_{\text{loop configs.}} n^L K^E \quad (4.1)$$

where L is the total number of loops and E the total number of loop edges. The qualitative phase diagram of this model is displayed in Fig. 8. The model undergoes various phase transitions within the range $-2 \leq n \leq 2$, in which we parametrize $n = 2 \cos \pi e$, $0 \leq e \leq 1$. It has *three* critical curves (represented as a zig-zag thick line and a thick straight line), characterized by the density of loops being either 0, between 0 and 1 or 1, respectively called dilute, dense and fully-packed phase. The latter case corresponds to a situation where the lattice is maximally occupied by loops, namely each vertex is visited by a loop, and it is obtained in the limit $K \rightarrow \infty$. The three critical curves are respectively described by CFT's with respective central charges [35] [36] [37]

$$\begin{aligned} \text{dilute} : c &= 1 - 6 \frac{e^2}{1+e} \\ \text{dense} : c &= 1 - 6 \frac{e^2}{1-e} \\ \text{fully - packed} : c &= 2 - 6 \frac{e^2}{1-e} \end{aligned} \quad (4.2)$$

It is beyond the scope of these notes to explain in detail these three formulas. They involve the so-called Coulomb gas description of the various critical theories, namely a description involving scalar free fields, each contributing 1 to the central charge, while a suitably defined background electric charge accounts for the contribution proportional to

e^2 . Typically, these scalar fields are the continuum limit of discrete “height variables” describing the degrees of freedom of the original model. In the case of loops, one may indeed define a dual height variable as follows. We first orient the loops arbitrarily, and then define a height variable as constant within each domain delimited by loops, and increasing or decreasing by a fixed amount when one goes across a loop pointing to the left or right (in other words, the loops form a contour plot of the height variable). This explains at least vaguely why only one scalar field will in general be sufficient to give a complete description of loop models. The background electric charge is also easy to understand as follows. To produce the correct weight $n = 2 \cos \pi e$ per loop, one simply attaches a weight $e^{\pm i\pi e}$ for each orientation. In turn, this is obtained by simply introducing a local weight $e^{\pm i\pi e/6}$ on each vertex visited by a loop, according to whether the loop makes a left or right turn. Indeed, on the hexagonal lattice the total of left minus right turns is always ± 6 , and the weight n per loop follows from the summation over all loop orientations. Now if we try to make sense of the loop model in a cylindric geometry, we see that if a given loop winds around the cylinder, it will have as many left and right turns, hence receive a wrong weight 2 instead of n . This is repaired by adding the background electric charge, which modifies the free field action and restores the correct weight, while modifying the central charge accordingly.

The fully-packed case is clearly distinguished in that it requires *two* scalar fields, rather than just one for the two other cases. More precisely, the central charge for fully-packed loops is exactly *one more* than that of the dense loops for the same value of n . Let us show in the two particular cases $n = 1, 2$ where this extra degree of freedom comes from.

The case $n = 1$ describes various equivalent problems for which configurations are depicted in Fig. 9: (i) rhombus tiling of the plane (ii) groundstates of the antiferromagnetic Ising model on the triangular lattice (iii) fully-packed loops on the honeycomb lattice. The interpretation (i) allows to immediately understand why the central charge $c = 1$ in this case. Indeed, the rhombus tiling may also be regarded as a view in perspective of the interface between two media, made of the piling-up of cubes. The natural height variable for this problem is simply the actual height of the various cubes, which in the continuum becomes the z coordinate of some landscape.

The case $n = 2$ may be interpreted as the problem of “phantom folding” of the 2D triangular lattice [38]. We start from the triangular lattice, viewed as a surface, namely

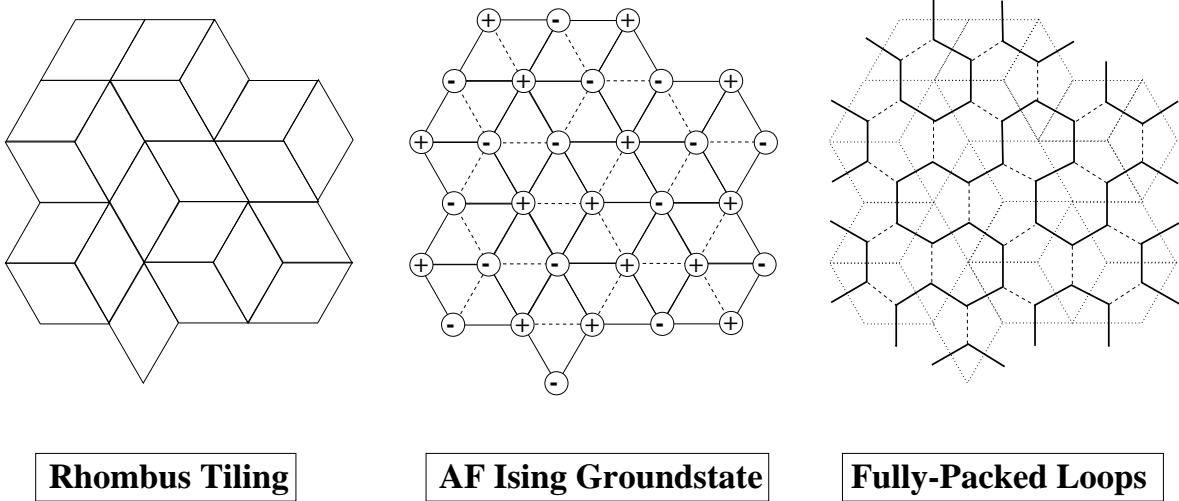


Fig. 9: Various interpretations of the fully-packed loop model's configurations on the hexagonal lattice: (i) rhombus tiling, obtained via the dual of the hexagonal lattice, the triangular lattice, in which we erase the edges dual to unoccupied edges, thus forming rhombi, which come in three possible orientations. (ii) Antiferromagnetic groundstates of the Ising model: one tries to maximize the number of antiferromagnetic interactions $(+-)$ between neighboring spins on the triangular lattice. Exactly one third of the edges remain frustrated (dashed here) namely are adjacent to equal spins: these frustrated edges of the triangular lattice are nothing but the erased ones in the rhombus tiling. (iii) Fully-packed loops on the hexagonal lattice: each vertex is visited by exactly one loop.

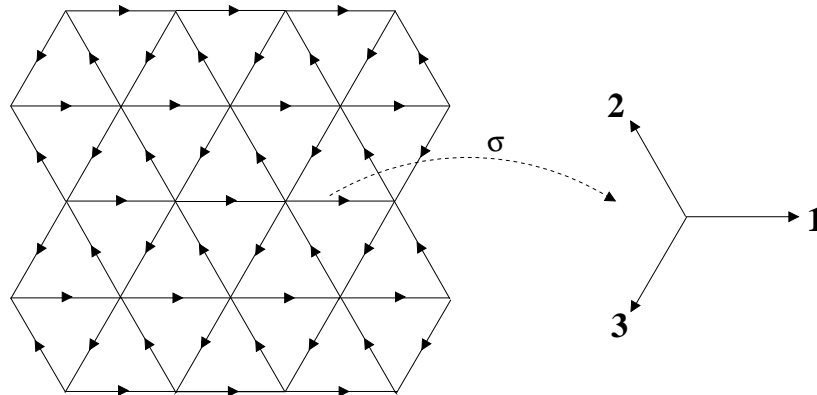


Fig. 10: The triangular lattice is represented as a surface, with edges viewed as tangent vectors (orientations are indicated by arrows), such that the sum over edges around each face vanishes $\sum_{\text{face}} \vec{e}_i = \vec{0}$. A phantom folding map σ is simply a map sending tangent vectors to either of the three images 1, 2, 3 that we have represented. This image is simply the value of the tangent vector in the folded configuration. As such, it must satisfy the face-rigidity constraint that $\sum_{\text{face}} \sigma(\vec{e}_i) = \vec{0}$.

with edges drawn as tangent vectors \vec{e} , in such a way that the sum of tangent vectors around each face vanishes (see Fig. 10), namely

$$\sum_{e \text{ around face } f} \vec{e} = \vec{0} \quad (4.3)$$

A phantom folding configuration is simply a configuration of this surface after being folded back to the plane, in a process where faces are not deformed, and edges serve as hinges between adjacent triangles. We are however interested only in the final folded states, not in their realizability with an actual material such as a piece of paper. It means that some of the foldings we consider may require cutting the sheet and letting it cross itself, hence the name phantom. More precisely, a folding map σ simply sends each edge \vec{e} to its new value in the folded configuration $\sigma(\vec{e})$. Finally the face-rigidity constraint turns into

$$\sum_{e \text{ around face } f} \sigma(\vec{e}) = \vec{0} \quad (4.4)$$

It is easy to see that the images $\sigma(\vec{e})$ may only take one of three possible values, denoted 1, 2, 3 in Fig. 10, namely the three unit vectors with vanishing sum (up to a global rotation). This allows to replace any phantom folding configuration by an edge tricoloring configuration of the triangular lattice, in which we paint edges with colors 1, 2, 3 in such a way that the three edges adjacent to each face have distinct colors. Representing the dual of such a configuration, we obtain an edge-tricoloring of the hexagonal lattice. Let us concentrate on the edges colored 1 and 2. It is easy to see that edges of alternating colors 1, 2, 1, 2, 1, 2... form fully-packed loops on the hexagonal lattice. Now exchanging the colors $1 \leftrightarrow 2$ along any of these loops independently also produces an admissible and distinct edge-tricoloring. This shows that the fully-packed loops receive naturally a weight $n = 2$ per loop. Finally picking arbitrarily the edges of color 3 in such a way that there be exactly one per vertex allows to generate all fully-packed loop configurations. We therefore end up with the fully-packed loop model on the hexagonal lattice, with $n = 2$. The height variable of the folding model is easily identified as the actual coordinate \vec{h} (in \mathbb{R}^2) of the vertices in the folded configurations. Being two-dimensional, these give naturally rise to *two* component scalar fields in the continuum, which explains the central charge $c = 2$ in this case (no background charge is necessary as there are no specific left/right turn weights). Note that the edge-tricoloring problem of the hexagonal lattice was solved by Baxter [39] by Bethe Ansatz techniques, and the central charge $c = 2$ may be directly extracted from

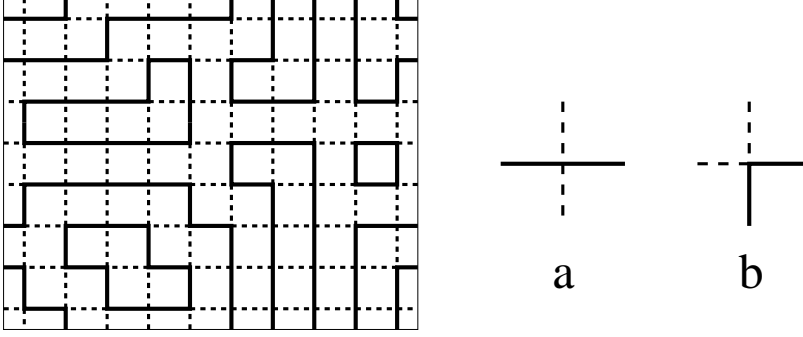


Fig. 11: A typical Fully-Packed loop configuration on the square lattice. Assuming doubly periodic boundary conditions, there are 6 black loops (solid line) and 4 white ones (dashed lines). Up to rotations, the vertices of the model are of the two types (a) “crossing” or (b) “tangent”.

that solution. The general fully-packed result (4.2) was derived by analogous techniques in [37].

Let us also mention another interesting loop model, which will eventually allow us to solve the meander problem: the two-flavor loop model on the square lattice. The configurations of this model are made of loops of *two* colors (flavors) say 1, 2 (or black, white) occupying edges of the square lattice, themselves belonging to at most one loop. The new condition is that although these loops are self-avoiding, two loops of distinct colors may coexist at a given vertex, by either crossing one-another, or being “tangent to one-another” as displayed in Fig. 11 (a) and (b). The model is further defined by attaching a weight K_i per edge occupied by a loop of color $i = 1, 2$ and n_i per loop of color $i = 1, 2$. The partition function of this model reads:

$$Z(n_1, n_2; K_1, K_2) = \sum_{\text{loop configs.}} n_1^{L_1} n_2^{L_2} K_1^{E_1} K_2^{E_2} \quad (4.5)$$

where L_i is the total number of loops of color $i = 1, 2$ and E_i the total number of edges in the loops of color $i = 1, 2$. In a way similar to the hexagonal lattice case, the model undergoes a number of interesting phase transitions, and in particular it still has a dense critical line, as well as a fully-packed one, for $-2 \leq n_1, n_2 \leq 2$, which we still parametrize by $n_i = 2 \cos \pi e_i$, $0 \leq e_i \leq 1$, $i = 1, 2$. The fully-packed constraint restricts the model to only configurations where all vertices are visited by the two types of loops, which corresponds to taking $K_1, K_2 \rightarrow \infty$ (see Fig. 11 for an example). This model is referred to as the FPL² model in the following. As before, Coulomb gas techniques have been used to identify

precisely the universality classes of the various critical models, leading in particular to formulas for the central charge of the underlying CFT [40]:

$$\begin{aligned} \text{dense} : c &= 2 - 6 \left(\frac{e_1^2}{1 - e_1} + \frac{e_2^2}{1 - e_2} \right) \\ \text{fully - packed} : c &= 3 - 6 \left(\frac{e_1^2}{1 - e_1} + \frac{e_2^2}{1 - e_2} \right) \end{aligned} \tag{4.6}$$

hence we still have an increase of $+1$ in the central charge when going from the dense to the fully-packed case at fixed n_1, n_2 . Again, the 2 and 3 in the central charges correspond to the number of degrees of freedom necessitated by the field theoretical description of the continuum limit, while the other contributions come from background charges which ensure the correct weights n_i per loop of color i in cylindric geometries. Let us now show where the three scalar fields come from in the fully-packed case.

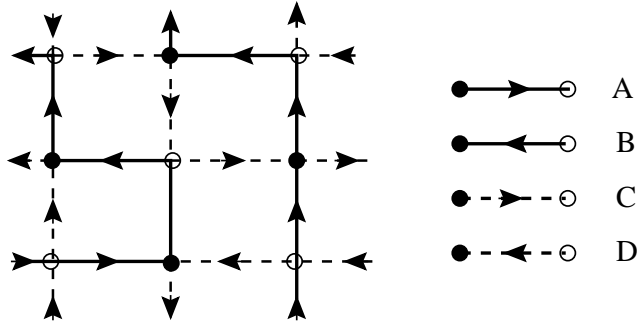


Fig. 12: A typical configuration of the FPL^2 model together with the bicoloration of its vertices (checkerboard of filled (\bullet) and empty (\circ) dots). We have added the corresponding dictionary that allows to map the loop configurations onto A, B, C, D labelings of the edges.

To do this, let us rephrase the model as a (3D) height model as follows. Starting again from an *oriented* fully-packed black and white loop configuration, we first *bicolor* the vertices of the square lattice, say with alternating filled (\bullet) and empty (\circ) dots. Then we use the dictionary of Fig.12 to assign one of the four labels A, B, C, D to each colored and oriented edge. With this convention, it is clear that edges of type $ABAB\dots$ alternate along black loops, whereas edges of type $CD CD\dots$ alternate along white loops, and that each vertex has one incident edge of each type A, B, C, D . It is clear that the four-labeling with A, B, C, D is in one-to-one correspondence with the coloring *and* orientation of edges

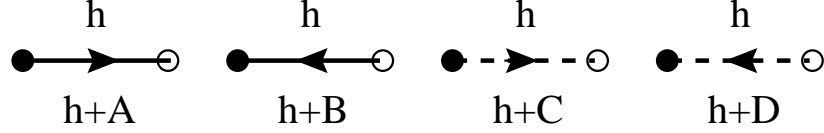


Fig. 13: Rules determining the change of the height variable across labeled edges. We adopt the Ampère convention that the height is increased (resp. decreased) by the edge value if the arrow of the edge points to the left (resp. right). The edge labels must be interpreted as three-dimensional vectors with the respective values \mathbf{A} , $-\mathbf{B}$, \mathbf{C} , $-\mathbf{D}$

of the FPL model. In particular, the orientation of a given black or white loop is reversed if we interchange the A and B or C and D labels along the loop.

The above colors allow for defining a dual vector height variable on the center of each face of the lattice. Indeed, viewing as vectors the A, B, C, D labeling of the edges of the lattice, let us arbitrarily fix the height to be zero on a given face of the lattice, and define it on all faces by successive use the rules of Fig.13 for the transition from a face to any of its neighbors. Note that it is necessary to impose the condition $\mathbf{A} + \mathbf{B} + \mathbf{C} + \mathbf{D} = 0$ to ensure that the heights are consistently defined around each vertex. We may therefore assume in all generality that $\mathbf{A}, \mathbf{B}, \mathbf{C}, \mathbf{D}$ are actually four vectors in \mathbb{R}^3 with vanishing sum; let us take for definiteness $\mathbf{A}, \mathbf{B}, \mathbf{C}, \mathbf{D}$ to be the four unit vectors pointing from the center of a tetrahedron towards its vertices. The heights are then clearly three-dimensional, as linear combinations of $\mathbf{A}, \mathbf{B}, \mathbf{C}, \mathbf{D}$.

To conclude this section, we have presented two types of loop models on the hexagonal and square lattice and studied their critical lines. In both cases, the fully-packed phase is described by *one more* scalar field than the dense one, resulting in an increase of $+1$ in the CFT's central charge.

4.3. Fully-packed loop models and 2DQG

In the next section, we will show how meanders may be viewed as configurations of the two-flavor loop model on a random lattice. To pave the road for further results, let us first consider here the ordinary (one-flavor) loop model on a random (trivalent) lattice.

Let us go back for a while to the fully-packed loop model with $n = 2$, interpreted above as the model of phantom folding of the triangular lattice. Recall that in that case the height variable has been identified with the position in \mathbb{R}^2 of the vertices in the folded configuration. We wish now to define this model on a *random triangulation*. For this to make sense, we need the triangulation to be foldable. Indeed, if it is not, the height variable

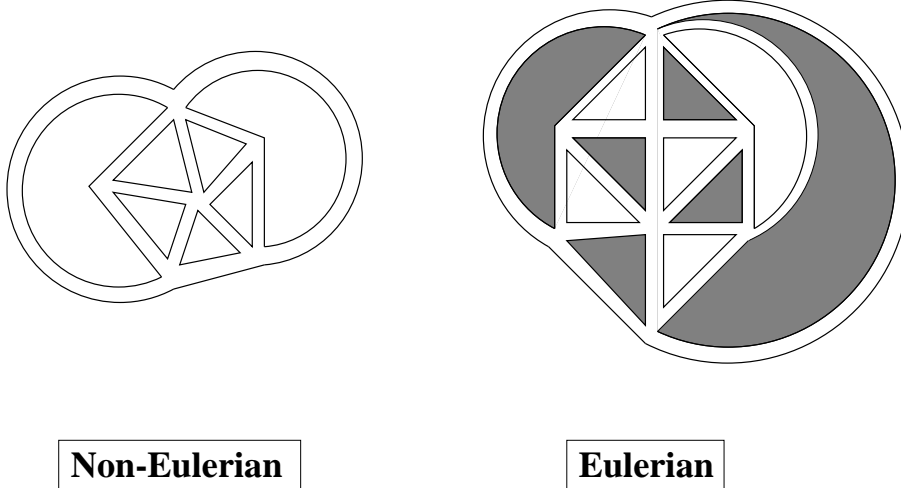


Fig. 14: Sample configurations of a planar non-Eulerian triangulation, and a planar Eulerian one. The Eulerian triangulation has only vertices of even valence, which allows to bicolor the triangular faces as shown.

can no longer be defined as the (2D) position in the folded configuration, but rather like in the dense case by viewing the loops as a contour plot for the (1D) height. In genus 0, the foldability amounts to the fact that each vertex is adjacent to an *even* number of triangles. In other words, the triangulation may be *bicolored*. Such a triangulation is also called Eulerian, as this guarantees the existence of an Eulerian path, visiting all triangles of the triangulation. Sample Eulerian and non-Eulerian triangulations are depicted in Fig. 14 for illustration. Summing over such triangulations will be called Eulerian gravity for obvious reasons. Now we may define two possible “gravitational” models of fully-packed loops on random trivalent graphs.

- We may sum over **arbitrary** trivalent graphs. As the dual triangulation will in general *not* be Eulerian, it will not be foldable, and the extra degree of freedom will be lost. The string susceptibility of the corresponding gravitational model (with as usual a weight g per trivalent vertex) will be computed using (2.7) with the dense central charge

$$\text{ordinary gravity : } c = 1 - 6 \frac{e^2}{1 - e}, \quad n = 2 \cos \pi e \quad (4.7)$$

- We may sum over **bipartite** trivalent graphs, whose dual triangulation is automatically foldable, thus preserving the height variable in \mathbb{R}^2 . The string susceptibility must be computed using (2.7) with the fully-packed central charge

$$\text{Eulerian gravity : } c = 2 - 6 \frac{e^2}{1 - e}, \quad n = 2 \cos \pi e \quad (4.8)$$

So we expect here a phenomenon very similar to that occurring in the case of hard particles. The universality class of the critical point depends crucially on the colorability property of the underlying random lattices. This similarity is no coincidence, as the very existence of *completely folded* groundstates relies crucially on the bipartiteness of the lattice just like the crystalline groundstates of the hard-particle model did.

To make the above argument even more solid, let us give a matrix model derivation of the results (4.7) and (4.8) in the case $n = 1$. The fully-packed model on random trivalent graphs is described by the partition function

$$Z(g) = \int dA dB e^{-N \text{Tr}(\frac{A^2}{2} + \frac{B^2}{2} - gAB^2)} \quad (4.9)$$

where as in Sect. 3.2 we use matrix elements of A and B , two $N \times N$ Hermitian matrices, to generate empty (resp. occupied) half-edges glued into empty (resp. occupied) edges via the propagators $\langle AA \rangle$ and $\langle BB \rangle$. Note that the measure of integration in (4.9) is normalized in such a way that $Z(g = 0) = 1$. As now usual, $\text{Log } Z(g)$ generates a sum over connected trivalent fatgraphs decorated by fully-packed loops of B matrix elements. We have $n = 1$, as there is no extra weight per loop. Noting that the dependence of $Z(g)$ on A is Gaussian, we may explicitly integrate over A , with the result:

$$Z(g) = \int dB e^{-N \text{Tr}(\frac{B^2}{2} - 2g^2 \frac{B^4}{4})} \quad (4.10)$$

As we already mentioned in Sect. 3.2, this latter integral simply generates random *quadrangulations*, therefore is a model of pure gravity with no matter, i.e. with $c = 0$, corresponding to the dense formula (4.7), with $n = 1$, $e = 1/3$.

To generate bipartite trivalent graphs (dual to Eulerian triangulations), we must use *complex* matrices A, B , whose pictorial representation bears an extra orientation, to distinguish between A and A^\dagger . The matrix integral for the fully-packed loop model on bipartite trivalent graphs reads [41]

$$Z_E(g) = \int dA dB e^{-N \text{Tr}(AA^\dagger + BB^\dagger - g(AB^2 + A^\dagger(B^\dagger)^2))} \quad (4.11)$$

where A and B are complex $N \times N$ matrices, and the measure is normalized in such a way that $Z_E(g = 0) = 1$. We note that the dependence on A is still Gaussian, hence upon integrating it out, we get

$$Z_E(g) = \int dB e^{-N \text{Tr}(BB^\dagger - g^2 B^2 (B^\dagger)^2)} \quad (4.12)$$

This turns out to be a particular case of the six-vertex model coupled to 2DQG solved in [42]. The corresponding central charge is $c = 1$, thus confirming the formula (4.8) at $n = 1$, $e = 1/3$.

The lesson to be drawn from this section is simple: the extra degree of freedom of the fully-packed loop model is wiped out if we are not careful enough with the type of random lattices we sum over. Only if these are bipartite will the height variable survive and lead eventually to the central charge (4.8). Otherwise, the mismatch between the random lattices and the model takes the universality class back to that of the dense model. We expect this result to be quite general and we will apply it in the next section to the case of the two-flavor fully-packed loop model on random tetravalent graphs.

4.4. From fully-packed loops on the square lattice to meanders

We are now ready to turn to the meander problem. It is by now clear that a meander configuration is nothing but a configuration of the two-flavor loop model on a random tetravalent graph, with in addition exactly *one* loop of each color, say the river (color 1) and the road (color 2). This assumes that we have closed the river (infinite line) into a loop as well. The operation of cutting the river loop and extending it into a line is equivalent to a marking (rooting) of the corresponding diagram, and yields an overall factor of $4n$ for diagrams with $2n$ vertices. In the language of the two-flavor fully-packed loop model, extracting the configurations with one loop of each color corresponds to letting $n_1, n_2 \rightarrow 0$, in order to select the leading contribution to the partition function, proportional to $n_1 n_2$ in this limit. But why at all consider the FPL^2 model? Indeed, only the “crossing” vertex of Fig. 11 (a) occurs in a meander configuration. The problem is that a two-loop flavor model on the square lattice with only the crossing vertex allowed is trivial, as loops should all be straight lines (closed into loops say by periodic boundary conditions). It simply means that the degrees of freedom of the lattice version of the meander model are not taken into account by this naive definition. We will show that the FPL^2 model provides the correct lattice version of the meander model.

Let us now study the FPL^2 model coupled to 2DQG, namely defined on random tetravalent graphs. As explained in Sect. 2, the genus zero partition function for this model reads

$$Z(n_1, n_2; g, x, y) = \sum_{\substack{\text{tetravalent planar} \\ \text{graphs } \Gamma}} \frac{1}{|\text{Aut}(\Gamma)|} \sum_{\substack{\text{FPL configs.} \\ \text{on } \Gamma}} n_1^{L_1} n_2^{L_2} (gx)^{V_a(\Gamma)} (gy)^{V_b(\Gamma)} \quad (4.13)$$

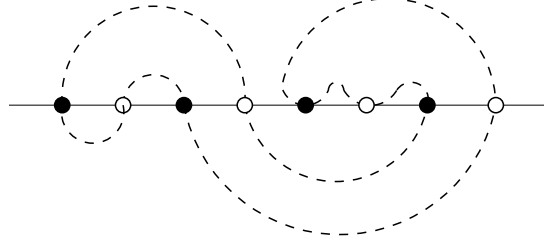


Fig. 15: A sample bipartite tangent meander with 8 vertices, among which 6 are crossing vertices (bridges) and 2 are tangency vertices. The vertices are bicolored, and all river or road edges connect only vertices of distinct colors.

where the sum extends over all planar four-valent graphs Γ , and $|\text{Aut}(\Gamma)|$ is the order of the symmetry group of Γ , while we have also denoted by V_a, V_b the total numbers of vertices of type a and b defined in Fig. 11 in the particular loop configuration, namely we have weighted each crossing of a black and a white loop by gx and each tangency by gy . From the lesson of Sect. 4.3, we know that if we wish to preserve all degrees of freedom of the model, we must couple it to Eulerian gravity, namely consider it on *bipartite* random tetravalent graphs in the sum (4.13) (we will distinguish this particular summation by an index E for Eulerian in the notation for the partition function). Indeed, recall that the definition of the (3D) height variable in Sect. 4.2 has relied crucially on the preliminary bicolouration of vertices of the lattice, allowing for defining the edge variables A, B, C, D . We may therefore use (4.13) to generate “bipartite tangent meanders”, namely configurations of a closed road crossing or tangent to a river (infinite line) through a given number of bicolored points $2n$, such that only points of distinct color are connected by river or road edges. Let μ_{2n} denote the number of bipartite tangent meanders with $2n$ vertices (see Fig. 15 for an illustration). These are well enumerated by counting configurations of the FPL² model at $n_1 = n_2 = 0$, namely $e_1 = e_2 = 1/2$, and by taking $x = y = 1$ in (4.13). More precisely, we have

$$\lim_{n_1, n_2 \rightarrow 0} \frac{1}{n_1 n_2} (Z_E(n_1, n_2; g, 1, 1) - 1) = \sum_{n \geq 1} \frac{\mu_{2n}}{4n} g^{2n} \quad (4.14)$$

where we have expressed that the opening of the river into an infinite line amounts to the marking of a river edge, and results in a factor $4n$ between the fixed n free energy f_{2n} and the tangent meander number μ_{2n} . Plugging the values $e_1 = e_2 = 1/2$ into the formula (4.6) and using (2.7), we find

$$c = -3 \quad \gamma_{str} = -\frac{1 + \sqrt{7}}{3} \quad (4.15)$$

The free energy at fixed area A for this model is nothing but

$$F_A = \frac{\mu_A}{2A} \sim \frac{g_c^{-A}}{A^{3-\gamma_{str}}} \quad (4.16)$$

by directly applying (2.10). Note that the value of g_c is not predicted by this argument, only the configuration exponent. We finally deduce the large n asymptotics of the bipartite tangent meander numbers

$$\mu_{2n} \sim \frac{g_c^{-2n}}{n^\beta} \quad \beta = \frac{7 + \sqrt{7}}{3} \quad (4.17)$$

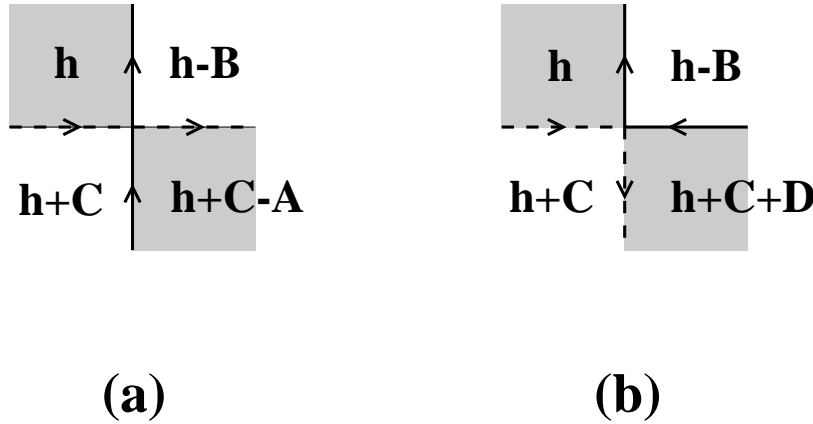


Fig. 16: Typical height configurations around (a) a crossing vertex and (b) a tangency vertex. When going diagonally say from the NW to the SE face (shaded), the height increases by an amount restricted to $\pm(\mathbf{A} - \mathbf{C})$, $\pm(\mathbf{B} + \mathbf{C})$ in the case (a) and only to $\pm(\mathbf{A} + \mathbf{B})$ in the case (b). Forbidding (b) will therefore amount to a reduction of the height variable range from 3 to 2 dimensions.

This is not however the end of the story. Indeed, the numbers μ_{2n} might have nothing to do with the meander numbers M_{2n} . We must examine more closely the role of the tangency points. Note that the meander numbers are correctly generated by taking $n_1, n_2, y \rightarrow 0$ in (4.13):

$$\lim_{n_1, n_2 \rightarrow 0} \frac{1}{n_1 n_2} (Z_E(n_1, n_2; g, 1, 0) - 1) = \sum_{n \geq 1} \frac{M_{2n}}{4n} g^{2n} \quad (4.18)$$

which just amounts to forbidding the tangency vertex b of Fig. 11. Forbidding the tangency vertex b will further restrict the range of the height variable of the model. In Fig. 16, we have displayed typical height configurations around a type a and a type b vertex for

comparison. It is easy to see that the increase in height when going diagonally from a face to another through the vertex (shaded faces in Fig. 16), there is more freedom at the crossing vertex a , where we may have $h \rightarrow h \pm (\mathbf{A} - \mathbf{C})$ or $h \pm (\mathbf{B} + \mathbf{C})$, while at the tangent vertex b we may only go in one spatial direction $h \rightarrow h \pm (\mathbf{A} + \mathbf{B})$. Forbidding the b vertex therefore has the net effect of dimensionally reducing the range of the height variable to only *two* dimensions rather than three in the full model. Forbidding tangencies therefore takes the central charge back to the dense value, which for $e_1 = e_2 = 1/2$ reads

$$c = -4 \quad \Rightarrow \quad \gamma_{str} = -\frac{5 + \sqrt{145}}{12} \quad (4.19)$$

Finally, using (4.18) and applying (2.10), we get the following meander number asymptotics for large n

$$M_{2n} \sim \frac{g_c^{-2n}}{n^\alpha} \quad \alpha = \frac{29 + \sqrt{145}}{12} \quad (4.20)$$

To make the above argument more solid, let us present an alternative route leading to the result (4.19). We may have considered in (4.13) a summation over arbitrary (non-necessarily bipartite) tetravalent graphs. In this case, the bicolouration of vertices disappears, and we have therefore no way of distinguishing the vector labels \mathbf{A} and $-\mathbf{B}$ on one hand and \mathbf{C} and $-\mathbf{D}$ on the other hand. This amounts to imposing an extra condition

$$\mathbf{A} + \mathbf{B} = \mathbf{C} + \mathbf{D} = 0 \quad (4.21)$$

This is precisely the condition one would obtain by considering the dense two-flavor loop model on the square lattice. Indeed, we still have the dictionary of Fig. 12 for edge labels, but as more vertices are allowed, we get some extra conditions for the height variable to be well-defined. If we consider a vertex crossed by only a black or white loop we immediately see that (4.21) must be satisfied. This explains the reduction $3 \rightarrow 2$ in the expression for the dense central charge (4.6) compared to the fully-packed one, as the (2D) height is now a linear combination of \mathbf{A}, \mathbf{C} which we may choose to form an orthonormal basis of \mathbb{R}^2 . Hence the simple fact that we sum over arbitrary tetravalent graphs takes the universality class of the FPL² model back to that of the dense one. For $e_1 = e_2 = 1/2$, we find precisely the result (4.19).

We must now see where meanders fit into this picture. Recall that we still have at this point crossing and tangent vertices, but we have relaxed the constraint of bicolourability.

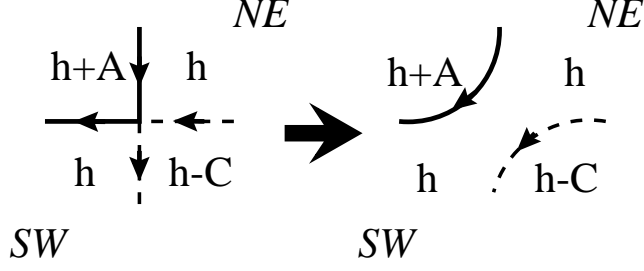


Fig. 17: A type b vertex of the FPL^2 model coupled to ordinary 2DQG, together with its dual height configuration. We note that the NE and SW heights are identical. We may therefore undo the vertex as shown, which explains its irrelevance.

We must again examine more closely the role of the tangency points. Forbidding them will yield the meander configurations as

$$\lim_{n_1, n_2 \rightarrow 0} \frac{1}{n_1 n_2} (Z(n_1, n_2; g, 1, 0) - 1) = \sum_{n \geq 1} \frac{M_{2n}}{4n} g^{2n} \quad (4.22)$$

Examining the height variable of the dense model around a tangency vertex, we see that the height variable is the same in the faces lying outside of the two loops (see Fig. 17). This means simply that the tangency vertex is *irrelevant* in the ordinary gravity situation, namely that its presence or absence, although it might affect the precise value of g_c , doesn't affect the universality class, hence the configuration exponent is independent of y at $x = 1$ in (4.13). We therefore end up with the meander universality class, determined by (4.21).

Some important numerical checks of the results of this section have been carried out by use of Jensen's transfer matrix method [43], which consists in generating the meander or tangent meander or bipartite tangent meander configurations by applying a local "transfer matrix" along the river, which implements the addition of a new vertex to a previous state. The method is powerful enough to give very accurate values for the extrapolated configuration exponents, which all confirm the various results obtained above [44]. Note that these are somewhat contested in [45], however the discrepancy with the predicted exponents is extremely small and possibly due to subtleties with the large n corrections.

4.5. The meander universality class: asymptotics of meandric numbers

We have now identified the CFT underlying meanders, as the dense two-flavor loop model with $n_1 = n_2 = 0$ coupled to ordinary 2DQG. The complete knowledge of the conformal operator content of this CFT via the Coulomb gas picture gives access to a host of meandric numbers which we describe now.

The important operators for our present purpose are those identified as generating oriented river vertices, namely the operators ϕ_k (resp. ϕ_{-k}), $k = 1, 2, \dots$ which correspond to the insertion of a k -valent source (resp. sink) vertex from (resp. to) which k oriented river edges originate (resp. terminate). Using these, we may generate configurations in which the river may itself form a complicated though connected oriented planar graph with possibly loops and endpoints, either sources or sinks according to the operators. In the Coulomb gas picture, these operators create “magnetic” defect lines along which the height variable has discontinuities. The operator ϕ_k has conformal dimension [40]

$$h_k = \frac{k^2 - 4}{32} \quad (4.23)$$

$k = \pm 1, \pm 2, \dots$ When coupled to 2DQG, these operators get dressed (into Ψ_k) and acquire the dimension (2.8):

$$\Delta_k = \frac{\frac{1}{2}\sqrt{8 + 3k^2} - \sqrt{5}}{\sqrt{29} - \sqrt{5}} \quad (4.24)$$

As a preliminary remark, we note that $h_{\pm 2} = \Delta_{\pm 2} = 0$. $\Psi_{\pm 2}$ indeed corresponds to the marking of an edge of the river in meanders, and moreover such operators must go by source/sink pairs for the orientations of the pieces of river connecting them to be compatible. Applying (2.11) to the two-point correlator $\langle \Psi_2 \Psi_{-2} \rangle_A$ at fixed large area A , we find

$$\langle \Psi_2 \Psi_{-2} \rangle_A \sim \frac{g_c^{-A}}{A^{1-\gamma_{str}}} \quad (4.25)$$

while the meander counterpart (with a closed river) behaves as $M_A/(2A) \sim g_c^{-A}/(A^{3-\gamma_{str}})$. We see that the net effect of the insertion of the operators $\Psi_{\pm 2}$ is an overall factor proportional to A^2 , which confirms their interpretation as marking operators. These are very important to keep in mind, as they might be required to ensure source/sink balance in various river geometries.

We may now turn to the case of semi-meanders, namely meanders in which the river is a semi-infinite line around the origin of which the road may freely wind. Considering the point at infinity on the river as just another point, the semi-meanders may equivalently be viewed as meanders whose river is made of a segment. Sending one of the ends of the segment to infinity just resolves the winding ambiguities around both ends. Using the above river insertion operators, we immediately identify the generating function for semi-meanders as

$$\langle \Psi_1 \Psi_{-1} \rangle = \sum_{n \geq 1} \bar{M}_n g^n \quad (4.26)$$

Using again (2.11) and the explicit values of $\Delta_{\pm 1}$ via (4.24), we arrive at the large n asymptotics

$$\bar{M}_n \sim \frac{g_c^{-n}}{n^{\bar{\alpha}}} \quad \bar{\alpha} = 1 + 2\Delta_1 - \gamma_{str} = 1 + \frac{\sqrt{11}}{24}(\sqrt{5} + \sqrt{29}) \quad (4.27)$$

Note that we expect the value of g_c to be the *same* for meanders and semi-meanders, as both objects occur as thermodynamic quantities in the *same* effective field theory.

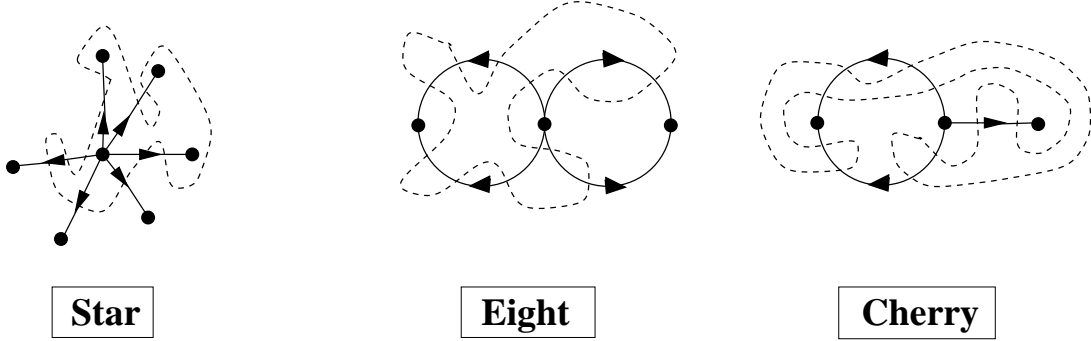


Fig. 18: Three types of meandric configurations in which the river has the geometry of (a) a k -valent star (b) an “eight” (c) a “cherry”. The vertices corresponding to river sinks or sources are represented by filled circles (\bullet). The edges of river inbetween them are oriented accordingly. The road (dashed line) may freely wind around univalent vertices.

We may now generate many more meandric numbers by considering more general correlators. To name a few (all depicted in Fig. 18), we may generate rivers with the geometry of a star with one k -valent source vertex and k univalent sink vertices generated by $\langle \Psi_k(\Psi_{-1})^k \rangle$, rivers with the geometry of an “eight” with one tetravalent source vertex and two loops, each containing a bivalent sink vertex generated by $\langle \Psi_4(\Psi_{-2})^2 \rangle$, or rivers with the geometry of a “cherry” with one trivalent source vertex, one univalent sink, and one loop, marked by a bivalent sink vertex generated by $\langle \Psi_3\Psi_{-1}\Psi_{-2} \rangle$, etc ... For each of these situations, we get the corresponding configuration exponent $\alpha = 3 - \gamma + \sum_i(\Delta_i - 1)$ by applying (2.11) with the dimensions (4.24). We get respectively

$$\begin{aligned} \alpha_{k\text{-star}} &= \frac{1}{48}(\sqrt{5} + \sqrt{29})(\sqrt{3k^2 + 8} + k(\sqrt{11} - 2\sqrt{29}) + 4\sqrt{29} - 2\sqrt{5}) \\ \alpha_{\text{eight}} &= \frac{1}{24}(\sqrt{5} + \sqrt{29})(\sqrt{14} + \sqrt{5}) \\ \alpha_{\text{cherry}} &= \frac{1}{48}(\sqrt{5} + \sqrt{29})(\sqrt{11} + \sqrt{35}) \end{aligned} \quad (4.28)$$

These values were also checked numerically in [44].

5. Conclusion

In these notes, we have tried to clarify the role of random lattices when coupling geometrically constrained systems such as hard particles or fully-packed loops to 2DQG. We have in both cases shown that the application of the famous KPZ formulas (2.7)(2.8) can be subtle, and involves the correct understanding of the models' degrees of freedom both on the fixed and random lattices. The main lesson is that if we want to preserve the essence (universality class) of a given model when coupled to 2DQG, then we must pay the price of restricting the fluctuations of space (random lattices) to those and only those preserving these degrees of freedom.

Provided we incorporate this lesson, we are free to use back and forth the KPZ formulas to transpose fixed lattice results into random lattice ones and vice versa. In the case of hard objects, we have used the 2DQG picture to infer some result on fixed lattices. In the case of fully-packed loops, we have used the opposite strategy to solve the meander asymptotics problem by using fixed lattice results on the dense or fully-packed two-flavor loop model. Along the way we have presented a number of other relations between fixed and random lattice models.

One could still wonder, now that we know the exact answers, whether one could devise some more rigorous mathematical proof of the various results inferred. In particular, the hard-triangle and hard-square models remain to be solved. As to meanders, the existence of a transfer matrix formulation may give some hope to be able to attain a combinatorial proof of our assertions. One could also wonder whether the recent combinatorial techniques for tackling planar graphs by use of trees might apply to meandric or loop problems (see [20] [46] [17] [18] for instance).

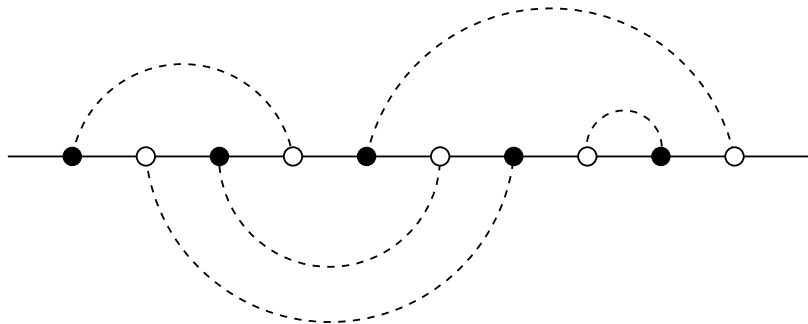


Fig. 19: A configuration of the one-flavor fully-packed loop model on a bipartite trivalent planar graph. We have opened the loop into a straight line and represented the unoccupied edges as dashed non-intersecting arches. Both loop and non-loop edges connect only vertices of distinct colors.

As a final question, let us mention the following simpler enumeration problem for which we also know the exact configuration exponent. It corresponds to the one-flavor fully-packed loop model coupled to Eulerian 2DQG, when $n \rightarrow 0$ [47]. The corresponding configurations are simply trivalent planar graphs with bicolored vertices and exactly one loop visiting all vertices. Upon opening the loop into an infinite line, we must enumerate planar configurations of non-intersecting arches connecting bicolored vertices on the line by pairs, in such a way that the colors of the connected vertices are always distinct (both along the river and along arches). A sample such configuration is depicted in Fig. 19. The resulting number of configurations for a fixed number $2n$ of vertices, ν_{2n} , counts also by duality the number of Eulerian triangulations with a Hamiltonian cycle. This number has the following large n asymptotics

$$\nu_{2n} \sim \frac{g_c^{-2n}}{n^\delta} \quad \delta = \frac{13 + \sqrt{13}}{6} \quad (5.1)$$

for some constant g_c . This is obtained by applying (2.10) with the string susceptibility (2.7) of the fully-packed loop model with $n = 0$ coupled to Eulerian gravity, namely with the fully-packed central charge (4.2) with $e = 1/2$, hence $c = -1$, and $\gamma_{str} = -\frac{1+\sqrt{13}}{6}$. Challenge: prove eqn. (5.1)!

References

- [1] J. Bouttier, P. Di Francesco and E. Guitter, *Critical and tricritical hard objects on bicolourable random lattices: exact solutions* J. Phys. A: Math. Gen. **35** (2002) 3821-3854.
- [2] P. Di Francesco, O. Golinelli and E. Guitter, *Meanders: exact asymptotics*, Nucl.Phys. B570 (2000) 699-712.
- [3] P. Di Francesco, *Folding and Coloring Problems in Mathematics and Physics*, Bulletin of the AMS, Vol. **37**, No. **3** (2000) 251-307.
- [4] D. Gaunt and M. Fisher, *Hard-Sphere Lattice Gases.I.Plane-Square Lattice*, J. Chem. Phys. **43** (1965) 2840-2863.
- [5] L. Runnels, L. Combs and J. Salvant, *Exact Finite Methods of Lattice Statistics. II. Honeycomb-Lattice Gas of Hard Molecules*, J. Chem. Phys. **47** (1967) 4015-4020.
- [6] R. J. Baxter, I. G. Enting and S.K. Tsang, *Hard Square Lattice Gas*, J. Stat. Phys. **22** (1980) 465-489.
- [7] P. Di Francesco, P. Mathieu and D. Sénéchal, *Conformal Field Theory*, Graduate Texts in Contemporary Physics, Springer (1996) 1-890 (1st ed.) and Springer (1999) 1-890 (2nd ed.).
- [8] A. Cappelli, C. Itzykson and J.-B. Zuber, *The A-D-E classification of minimal and $A_1^{(1)}$ conformal invariant theories*, Comm. Math. Phys. **113** (1997), 1-26.
- [9] P. Di Francesco, P. Ginsparg and J. Zinn-Justin, *2D Gravity and Random Matrices*, Physics Reports **254** (1995) 1-131.
- [10] R. J. Baxter, *Hard Hexagons: Exact Solution*, J. Phys. A **13** (1980) L61-L70; R. J. Baxter and S.K. Tsang, *Entropy of Hard Hexagons*, J. Phys. A **13** (1980) 1023-1030; see also R. J. Baxter, *Exactly Solved Models in Statistical Mechanics*, Academic Press, London (1984).
- [11] R. J. Baxter, *Planar Lattice Gases with Nearest-neighbour Exclusion*, Annals of Combin. No. **3** (1999) 191-203 preprint cond-mat/9811264.
- [12] D. Kurze and M. Fisher, *Yang-Lee Edge Singularities at High Temperatures*, Phys. Rev. **B20** (1979) 2785-2796.
- [13] J. Cardy, *Conformal Invariance and the Yang-Lee Edge Singularity in Two Dimensions*, Phys. Rev. Lett. **54**, No. 13 (1985) 1354-1356.
- [14] P. Di Francesco, *Matrix Model Combinatorics: Applications to Folding and Coloring*, Bleher and Its Eds., MSRI Publications Vol. **40** 111-170, Cambridge University Press (2001), math-ph/9911002.
- [15] B. Eynard, *Random Matrices*, Saclay Lecture Notes (2000), http://www-spht.cea.fr/lectures_notes.shtml
- [16] C. Itzykson and J.-B. Zuber, *The planar approximation II*, J. Math. Phys. **21** (1980) 411.

- [17] J. Bouttier, P. Di Francesco and E. Guitter, *Combinatorics of Hard Particles on Planar Graphs*, Saclay preprint t02/160 and cond-mat/0211168 (2002).
- [18] M. Bousquet-Mélou and G. Schaeffer, *The degree distribution in bipartite planar maps: applications to the Ising model*, preprint math.CO/0211070 (2002).
- [19] W. Tutte, *A Census of Planar Maps*, Canad. Jour. of Math. **15** (1963) 249-271.
- [20] G. Schaeffer, *Bijective census and random generation of Eulerian planar maps*, Electronic Journal of Combinatorics, vol. **4** (1997) R20; *Conjugaison d'arbres et cartes combinatoires aléatoires* PhD Thesis, Université Bordeaux I (1998).
- [21] V.G. Knizhnik, A.M. Polyakov and A.B. Zamolodchikov, *Fractal Structure of 2D Quantum Gravity*, Mod. Phys. Lett. **A3** (1988) 819-826; F. David, *Conformal Field Theories Coupled to 2D Gravity in the Conformal Gauge*, Mod. Phys. Lett. **A3** (1988) 1651-1656; J. Distler and H. Kawai, *Conformal Field Theory and 2D Quantum Gravity*, Nucl. Phys. **B321** (1989) 509-527.
- [22] P. Di Francesco, *Rectangular Matrix Models and Combinatorics of Colored Graphs*, preprints SPhT/02-096 and cond-mat/0208037 (2002), to appear in Nucl. Phys. **B**.
- [23] A. Sainte-Laguë, *Avec des nombres et des lignes (Récréations Mathématiques)*, Vuibert, Paris (1937).
- [24] J. Touchard, *Contributions à l'étude du problème des timbres poste*, Canad. J. Math. **2** (1950) 385-398; W. Lunnon, *A map-folding problem*, Math. of Computation **22** (1968) 193-199.
- [25] P. Di Francesco, O. Golinelli and E. Guitter, *Meander, folding and arch statistics*, Mathl. Comput. Modelling **26** (1997) 97-147.
- [26] V. Arnold, *The branched covering of $CP_2 \rightarrow S_4$, hyperbolicity and projective topology*, Siberian Math. Jour. **29** (1988) 717-726.
- [27] K.H. Ko, L. Smolinsky, *A combinatorial matrix in 3-manifold theory*, Pacific. J. Math **149** (1991) 319-336.
- [28] K. Hoffman, K. Mehlhorn, P. Rosenstiehl and R. Tarjan, *Sorting Jordan sequences in linear time using level-linked search trees*, Information and Control **68** (1986) 170-184.
- [29] P. Di Francesco, O. Golinelli and E. Guitter, *Meanders and the Temperley-Lieb Algebra*, Commun. Math. Phys. **186** (1997), 1-59.
- [30] R. Bacher, *Meander Algebras*, prépublication de l'Institut Fourier n° 478 (1999).
- [31] S. Lando and A. Zvonkin, *Plane and Projective Meanders*, Theor. Comp. Science **117** (1993) 227-241, and *Meanders*, Selecta Math. Sov. **11** (1992) 117-144.
- [32] P. Di Francesco, O. Golinelli and E. Guitter, *Meanders: a direct enumeration approach*, Nucl. Phys. **B 482** [FS] (1996) 497-535.
- [33] O. Golinelli, *A Monte-Carlo study of meanders*, Eur. Phys. J. **B14** (2000) 145-155.
- [34] Y. Makeenko *Strings, Matrix Models, and Meanders*, Nucl.Phys.Proc.Suppl. **49** (1996) 226-237; G. Semenoff and R. Szabo *Fermionic Matrix Models* Int.J.Mod.Phys. **A12** (1997) 2135-2292.

- [35] B. Nienhuis in *Phase Transitions and Critical Phenomena*, Vol. 11, eds. C. Domb and J.L. Lebowitz, Academic Press 1987.
- [36] H.W.J. Blöte and B. Nienhuis, Phys. Rev. Lett. **72** (1994) 1372.
- [37] M.T. Batchelor, J. Suzuki and C.M. Yung, Phys. Rev. Lett. **73** (1994) 2646, cond-mat/9408083.
- [38] P. Di Francesco and E. Guitter, *Entropy of Folding of the Triangular Lattice*, Europhys. Lett. **26** (1994) 455.
- [39] R. Baxter, *Colorings of a hexagonal lattice*, J. Math. Phys. **11** (1970) 784-789.
- [40] J. Jacobsen and J. Kondev, *Field theory of compact polymers on the square lattice*, Nucl. Phys. **B 532** [FS], (1998) 635-688, *Transition from the compact to the dense phase of two-dimensional polymers*, J. Stat. Phys. **96**, (1999) 21-48.
- [41] P. Di Francesco, E. Guitter and C. Kristjansen, *Fully Packed $O(n=1)$ Model on Random Eulerian Triangulations*, Nucl.Phys. B549 (1999) 657-667.
- [42] V. Kazakov and P. Zinn-Justin, *Two-Matrix model with ABAB interaction*, Nucl.Phys. **B546** (1999) 647-668.
- [43] I. Jensen, *Enumerations of Plane Meanders*, preprint cond-mat/9910313 (1999).
- [44] P. Di Francesco, E. Guitter and J. Jacobsen, *Exact Meander Asymptotics: a Numerical Check*, Nucl.Phys. B580 (2000) 757-795.
- [45] I. Jensen and A. Guttmann, *Critical exponents of plane meanders*, J. Phys. **A33** (2000) L187; I. Jensen, *A transfer matrix approach to the enumeration of plane meanders*, preprint cond-mat/0008178 (2000).
- [46] J. Bouttier, P. Di Francesco and E. Guitter, *Counting colored random triangulations*, Nucl. Phys. **B641**[FS] (2002) 519-532; *Census of Planar Maps: From the One-Matrix Model Solution to a Combinatorial Proof*, Nucl.Phys. **B645** (2002) 477-499.
- [47] E. Guitter, C. Kristjansen, and J. Nielsen, *Hamiltonian Cycles on Random Eulerian Triangulations*, Nucl.Phys. B546 (1999) 731.